SHEAR FRACTURE ON THE BASIS OF FRACTURE MECHANICS

SCHUBVERSAGEN AUF DER BASIS DER BRUCHMECHANIK

LA RESISTANCE AU CISAILLEMENT A LA BASE DE LA MECANIQUE DE RUPTURE

Shilang Xu, Hans W. Reinhardt

SUMMARY

The shear resistance of reinforced concrete beams is explained on the base of fracture mechanics. If one uses the stress intensive factor K_{II} one can predict the shear resistance of concrete. The formulas which are necessary to calculate the ultimate loads are given.

ZUSAMMENFASSUNG

Der Schubwiderstand von Trägern aus Stahlbeton wird auf der Basis der Bruchmechanik erklärt. Wenn man den Spannungsintensitätsfaktor K_{II} verwendet, kann man das Schubversagen vorhersagen. Die notwendigen Formeln zur Berechnung der Schubtragfähigkeit werden angegeben.

RESUME

La résistance au cissaillement des poutres en béton armé est expliqué à la base de la mécanique de rupture. Si on utilise le facteur K_{II} de la mécanique de rupture on peut prédire le resistance au cissaillement. Les formules pour calculer les forces ultimes sont données.

KEYWORDS: Shear, fracture mechanics, concrete, K_{II}, cracking

1. INTRODUCTION

In practical engineering, the shear failure is a fundamental problem. In a reinforced concrete beam, the shear force acted at a section is commonly taken by the concrete compress zone, the stirrups, the dowel action of the longitudinal reinforcement and the aggregate interlock in the crack. All sections of a beam are checked and reinforced according to the shear action. Nowadays, various empirical formulae to evaluate the shear loading capacity are given in different

design codes respectively that were developed using a regression analysis of experimental data. Even for the flexural-shear failure problem in the slender beams without stirrups, the empirical regression formulae are used in the design codes, no satisfactory physical model exists yet. In fact, the diagonal failure occurred in slender beams without stirrups is a typical brittle fracture, of which, the experimental results observably size effect. Therefore, several researchers attempted to apply fracture mechanics to the shear failure for gaining a satisfactory physical model of the shear failure. But, it is not clear that the shear stress component plays somehow a role in the shear failure due to the complication of the stresses distribution near the tip of the diagonal crack. In order that the shear crack propagation and shear fracture properties can be well understood, mode II testing needs to be performed for measuring mode II fracture toughness K_{IIc} and mode II fracture energy G_{IIF} of concrete materials. In practical engineering structures, there are some cases, for instances, the joints between dissimilar media under shear forces and normal forces parallel to the existing crack and doorcase in buildings under shear forces□where mode II prevails right from the crack propagation initiation. In such cases, the mode II fracture parameters can be directly applied to analysis.

In order to understand mode II fracture properties of concrete, it is necessary to perform mode II fracture tests on suitable specimen geometry. Many researchers have paid their attention on seeking mode II fracture tests without mode I component supplement. Some testing methods have been proposed and applied to various materials. Figure 1 shows eight specimen geometry and loading configurations which have been also applied to concrete. Figure 1a indicates the situation of pure shear stresses along a crack which is envisaged by testing but cannot be realized.

Figure 1b goes back to Iosipescu [1] who proposed this geometry for testing metals and welded joints. It looks very attractive and has been used by several researchers on concrete either with a single notch specimen or a double notch specimen [2-7]. The results and interpretations were rather controversial. After Barr and Derradj [8], Schlangen [9] came to the conclusion that mode I is the governing mode of this test. The push-off specimen of Figure 1c was proposed by Mattock and Hawkins [10] to investigate interfaces in reinforced concrete. Finite element analyses have shown that a tensile stress exists at the crack tip, which is of the same magnitude as the shear stress, that is, a mixed state of stress exists. A variation of the same idea has been realized by Nooru-Mohamed

[11]. The axisymmetric punch-through specimen (Figure 1d) has been analysed by Tada [12]. It has been used on mortar and concrete [13] due to its easy handing. However, numerical studies have shown that large tensile stresses occur at the crack tip. A recent study has shown that the tensile stresses can be reduced considerably by choosing four notches and by varying the depth of the notches [14].

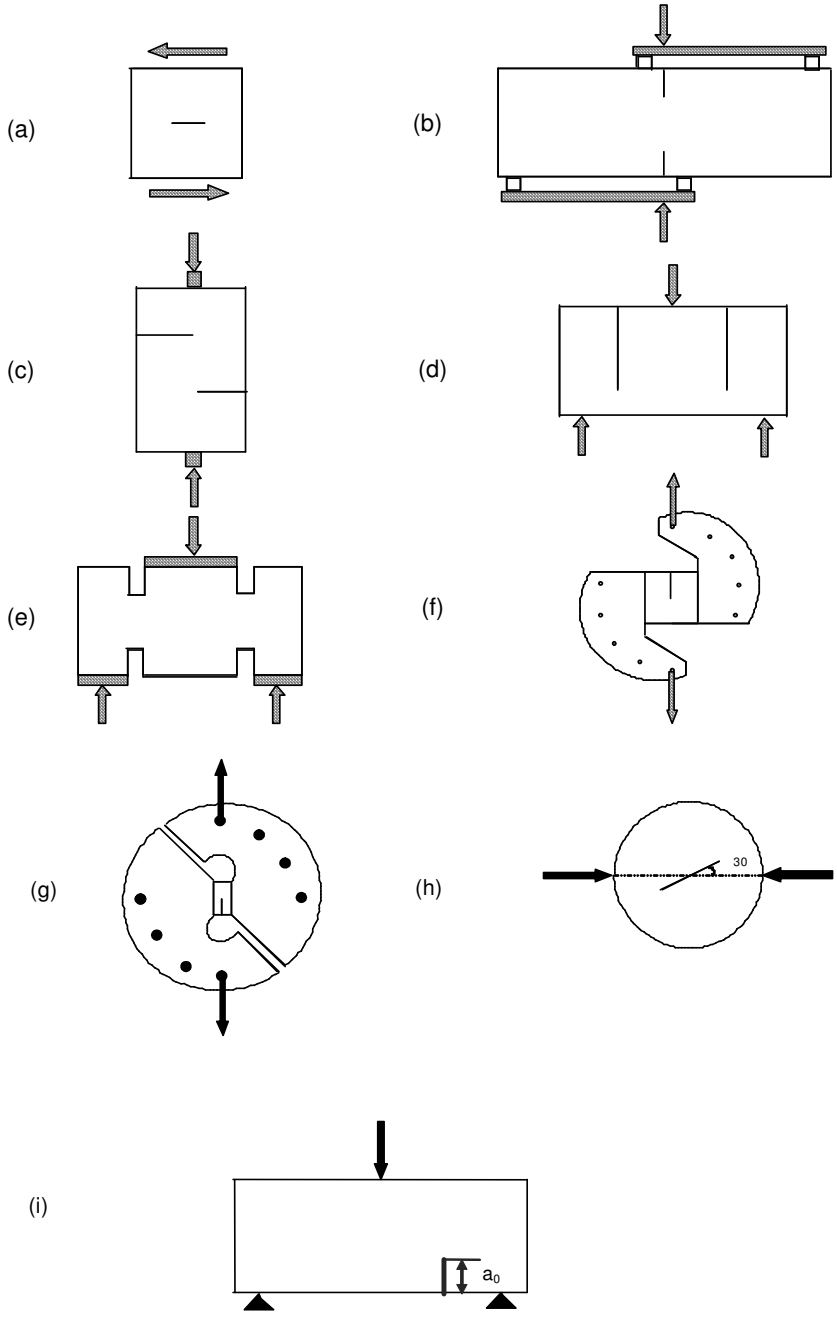

Figure 1. Different mode II testing configurations: (a) Schematic state of shear stresses along a crack; (b) Iosipescu specimen; (c) Push-off specimen; (d) Punch-through specimen; (e) Four-notch cylinder; (f) Mixed-mode device according to Richard; (g) Mixed-mode device according to Arcan; (h) Mixed-mode disk loading; and (i) Off-centre notched beam.

For rock core testing, the cylindrical specimen with four notches (Figure 1e) has been proposed by Luong [15] which yields mixed mode results. Figures 1f and 1g show elaborate testing devices which allow various mixed combinations by rotating the holder of the specimen. Both devices (Figure 1f, according to Richard [16], Figure 1g, according to Arcan [17]) are used in photo-elastic studies but not on concrete. Izumi et al. [18] have converted the device for compressive loading and applied to concrete in mixed mode loading. Due to compressive loading there is a negative K_I at the crack tip. Figure 1h has been proposed by Irobe and Pen [19] and also used by Jia et al. [20]. Finally, the off-centre notched beam specimen by Jenq and Shah [21] has been applied in a study on mixed mode fracture (Figure1i). More investigations on mode II fracture testing methods had been made [22-31].

Although there are several methods proposed for mode II testing, none of them produces a pure mode II situation. Either by eccentric loading or by deformation during testing, a mode I contribution cannot be avoided which make these testing arrangements mixed mode devices. It was the reason to carry out this research project to look for an improved testing method to study the pure shear fracture of concrete.

Recent years, many researchers have carried out mode II fracture tests on new specimen geometry, called double-edge notched specimen. The new specimen geometry and loading arrangement has firstly been applied to wood. For these highly orthotropic materials, the double-edge notched specimen has been subjected to tensile loading which enables to measure K_{IIc} and G_{IIF} in the direction normal to the grain (Xu, Reinhardt and Gappoev, 1996) [32].

Reinhardt, Ozbolt, Xu and Abebe (1997) [33] did not only measure K_{IIc} of high strength concrete using the same approach as the above mentioned, but they also carried out numerical studies on the double-edge notched specimen using the MASA Finite Element Program based on the microplane model. In 1998, the numerical studies on the mode II geometry were continuously enhanced (Ozbolt, Reinhardt and Xu)[34].

Cedolin, Bisi and Nardallo (1997) [35] performed experiments and a numerical study on the double-edge notched specimens too. Their numerical study confirmed that the formulae (1) and (2) apply to different half width of the tested specimen. They observed the crack propagation at the notch tip through moiré interferometry. The fact was confirmed that the initiation of crack propagation at

the notch tip corresponds with the discontinuity point of the load vs. displacement recorded. This discontinuity point is the critical mode II fracture point. According to the critical mode II fracture load they determined the mode II fracture toughness K_{IIc}. Then using the relation of $G = K^2/E$, they calculated the fracture energy G_{IIF}. In fact, their experimental arrangement could have been improved. The positions of two extensometers are too far from the notches because fracture is very localized. This could easily be affected by random noise (Cedolin et al. 1998)[36]. As the result, to determine the critical mode II fracture load on the recorded plots of load vs. displacement could become difficult. Later, Prisco and Ferrara (1998) [37] numerically studied the double-edge notched mode II specimen made of high strength concrete. They aimed to evaluate fracture energy. Their numerical results are in agreement with those achieved by Ozbolt et al. (1998)[34]. When Prisco and Ferrara [37] compared their numerical results with Cedolin et al.'s experimental ones, differences of both the concrete strength and the geometry sizes used in their numerical study and the experimental observation of Cedolin et al. (1997) [35] were ignored. This could be a reason that they questioned the experimental results of Cedolin et al. (1997) [35] in their conclusions. However, Prisco and Ferrara[37] provided numerical results in detail for this new mode II geometry in their work. Then, mode II fracture toughness K_{IIc} of normal strength concrete was realistically measured using tests on the double edge notched specimens by Reinhardt and Xu in 1998 [38].

Later, Reinhardt and Xu [39] used the double edge notched specimens and unnotched specimens to carry out mode II fracture tests and proposed a practical approach to determine mode II fracture energy G_{IIF} from the experiments for concrete materials.

In this chapter, we mainly introduce the mode II fracture testing on the double-edge notched specimens, the measurements of mode II fracture toughness K_{IIc} and mode II fracture energy G_{IIF} of concrete materials, mode II fracture properties and mode II crack propagation observed in experiments and in numerical simulation. In the final section, the fracture mechanics approach to predict the shear capacity of slender beams without stirrups proposed by other researchers is introduced too.

2. THE ANALYTICAL THEORIES FOR THE MODE II TESTING METHOD

2.1 The Double-Edge Notched Infinite Plate

The theoretical analysis was carried out to propose an improved testing method. The double-edge notched plate seems appropriate. Figure 2 shows the geometry of a double-edge notched infinite plate under in-plane tensile loading. For such a case in Figure 2 a plate with unit thickness is infinite both in x-direction and in y-direction. The length of ligament, 2*a*, in the plate is finite, but, the lengths of double-edge notches are infinite. Under the loading condition shown in Figure 2, Tada [12] solved this problem and gave the formulae of stress intensity factors as follows:

$$K_I = 0$$
$$K_{II} = \frac{\sigma}{4}\sqrt{\pi a} \tag{1}$$

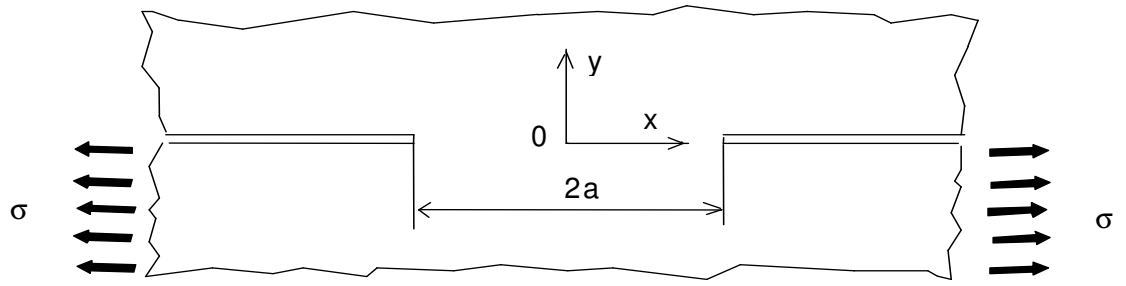

Figure 2. Double-edge notched infinite plate.1

It is important to notice that K_I *vanishes* and K_{II} remains as the only stress component. This theoretical solution is valid for an infinite plate and the question is whether it is also applicable to a specimen of finite size.

2.2 The Double-Edge Notched Plate of Finite Size

If the width of the plate in y-direction shown in Figure 2 is finite and is denoted with w, then, the problem becomes a double-edge notched infinite strip (see Figure 3). The stress intensity factor for such case shown in Figure 3 can be solved by methods of *J*-integral proposed by Rice [40].

If we take out a half of the strip, the stress distribution along the symmetry axis of the strip could be assumed to be linear distributions (see Figure 4). The *J*-integral had been stated by Radaj and Zhang [41] as in the following form:

$$J = \int_{\Gamma}(\tau_{xy} du + \sigma_y dv - W dy) \tag{2}$$

where

$$W = \frac{1}{2E}[\sigma_x^2 + \sigma_y^2 - 2ny \sigma_x \sigma_y + 2(1+ny)\tau_{xy}^2]$$

According to the relation between of J-integral and stress intensity factor we have

$$K_{II}^2 = JE \quad (for\ this\ case\ K_I = 0) \tag{3}$$

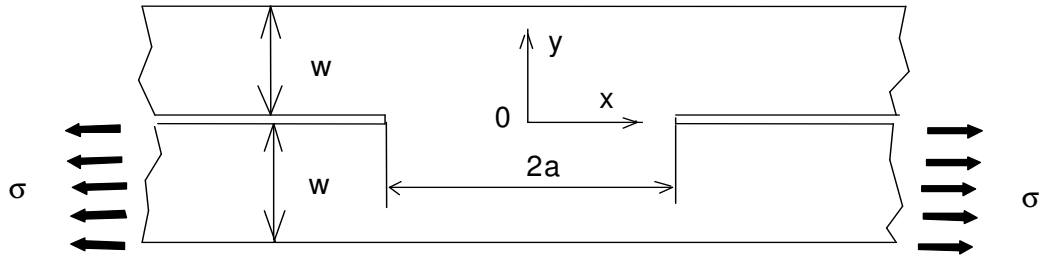

Figure 3. Double-edge notched infinite strip.

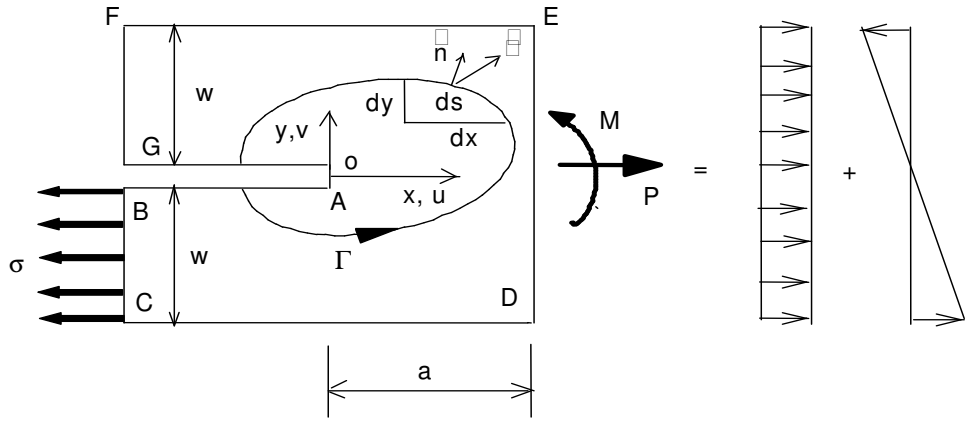

Figure 4. Integration path.

The *J*-integral is path independent. Hence, we can choose such an integral path:

$$J = \int_{AB} \cdots + \int_{BC} \cdots + \int_{CD} \cdots + \int_{DE} \cdots + \int_{EF} \cdots + \int_{FG} \cdots + \int_{GA} \cdots$$

along the contour lines *GA*, *AB*, *EF*, *CD*:

$$\int_{GA} \cdots = \int_{AB} \cdots = \int_{EF} \cdots = \int_{CD} \cdots = o \qquad (\sigma_y = o,\ \tau_{xy} = o,\ dy = o)$$

along the contour line *FG*:

$$\int_{FG} \cdots = o \ (\tau_{xy} = o,\ \sigma_x = o,\ \sigma_y = o)$$

Therefore

$$\begin{aligned} J &= -\left(\int_{BC} W\,dy + \int_{DE} W\,dy\right) \\ W &= \frac{\sigma_x^{\,2}}{2E} \quad (\sigma_y = \tau_{xy} = o) \end{aligned} \tag{4}$$

where along the *BC*: $\sigma_x = -\sigma$, and along the *DE*:

$$\sigma_x = \frac{\sigma}{2} - \frac{3\sigma}{4w} y$$

By submitting these relations to (4):

$$J = -\left[\int_{o}^{-w} \frac{\sigma^2}{2E}\,dy + \int_{-w}^{w} \frac{\left(\frac{\sigma}{2} - \frac{3\sigma}{4w} y\right)^2}{2E}\,dy\right] = \frac{\sigma^2 w}{16E} \tag{5}$$

Note with (3) we can get:

$$K_{II} = \frac{\sigma}{4}\sqrt{w} \tag{6}$$

The same numerical result has been achieved by various authors [42-45] who used other mathematical tools when they analyzed the contact problem of two perfectly bonded infinite strips of dissimilar materials. The special case of

the two equal materials and same width leads to (6) and $K_I = 0$. From [43] it is concluded that a finite length of the strip $h = 2a$ can be assumed to be infinite. Using this knowledge, new specimen geometry for pure shear testing can be designed. The length of the specimen h should be $= 2a$ in order to apply equation (6). Furthermore, for $h = 2a$ and $w = \pi a$ equation (1) applies.

2.3 Predicted Size Effect

Equations (1) and (6) are suited to predict a size effect. According to eq. (1), K_{II} increases with $a^{1/2}$, that is, if the ligament ($2a$) of one structure is twice the one of another structure, the stress needed to reach K_{IIc} is only $(1/2)^{1/2}$ as large. Figure 5 shows the relation between ligament and critical stress. This relation applies to an infinite plate.

On the other hand, if the infinite plate is reduced to an infinite strip with $2w$, eq. (6) does not show a dependence of the critical stress on the ligament length but only on the strip width. This means that the critical stress is constant for a constant w and varying ligament length. This is true until $w = \pi a$. Figure 6 shows the critical stress versus the ligament length for different strip widths.

The transition point shifts to the left with smaller width of the strip. Figure 6 shows that a size effect of the ligament length does only exist if $a = w/\pi$ (stable crack growth). The same have been shown by Ozbolt [46] for mode-I and mixed failure modes. Therefore, when judging a certain structure, the starting point in Figure 6 can lie on the curves line or on the horizontal line depending upon the combination of a and w.

There is a second feature of the double-edge notched plate which should receive attention. Equation (1) and (6) predict a critical stress for a certain K_{IIc}. If $K_{II} = K_{IIc}$ the crack (notch) will extend and, thus, the ligament length will decrease. As a consequence, the critical stress increases what means that $\sigma < \sigma_c$ and the situation is stable again. Figure 6 and eq. (6) predict that a crack will propagate until $a = w/\pi$ and that the crack arrests if the remote stress is kept constant. The crack propagates again only if the stress increases. This may lead to the situation that final shear failure will not occur but that other mechanisms govern the collapse for instance, compressive failure.

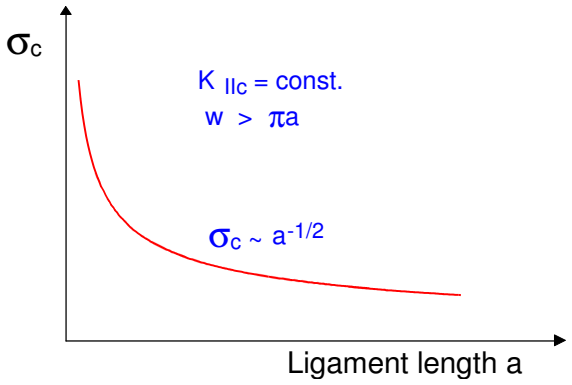

Figure 5. Influence of ligament length on critical stress.

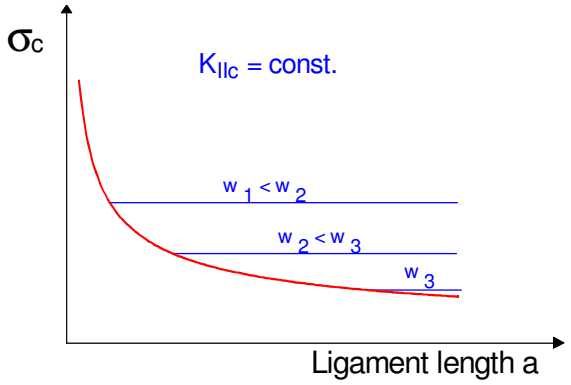

Figure 6. Critical stress versus ligament length and strip width.

3. NUMERICAL STUDY ON THE DOUBLE-EDGE NOTCHED SPECIMEN OF NORMAL STRENGTH CONCRETE FOR THE MODE II TESTING

The results gained using MASA FE-Program based on the microplane model proposed by Ozbolt et al. [47] in the numerical study are shown in this section for having a good understanding of the stress field distribution, strain field distribution as well as the failure pattern during the loading process. The loading arrangement and the specimen geometry used in the numerical study are shown in Figure 7. Herein, the specimen is 200 mm high, 200 mm wide and 50 mm thick and the notch is 50 mm long and 2 mm wide. The half width to subject compressive load is 99 mm. The compressive strength of concrete is 40 MPa, the tensile strength is 2.8 MPa, the modulus of elasticity is 32 GPa and the fracture energy in mode I is assumed 80 N/m. The relation of stress - strain in uniaxial tension is given in Figure 8 (a) and the one in uniaxial compression in Figure 8 (b).

In the calculation, the gained plot of load versus displacement for the specimen is shown in Figure 9. Through investigation of the stress field distribution, strain field distribution as well as the failure pattern during the loading process, we can observe whether shear fracture occurs along the ligament prior to the compressive failure in the loaded part, or opposite. Four typical loading stages are chosen and marked on Figure 9. The corresponding four typical loading stages are 83% of P_{max}; 92% of P_{max}; P_{max} and 92% of P_{max} post peak load. The lateral stresses distributions for the four loading stages are shown in Figure 10. The shear stresses distributions are given in Figure 11.

Then, the shear strain distributions and the principal strain distributions are presented in Figure 12 and 13 respectively. From Figure 12, it can be seen that high shear strains occur along the ligament. Prior to exceeding the peak load, the principal strains show the same distribution as the shear strains. It implied that the shear strains are mainly dominant in the principal strain distributions.

Importantly, the results gained in the numerical study show that the shear fracture along the ligament happened prior to the compressive failure in the loaded part. Figure 15 shows somehow softening of shear stress in the front of mode II crack. Combining Figures 10 and 11, one can find mode II crack propagation prior to exceeding the peak load. It provided a good proof for the testing determination of fracture energy G_{IIF} in mode II that will be presented later.

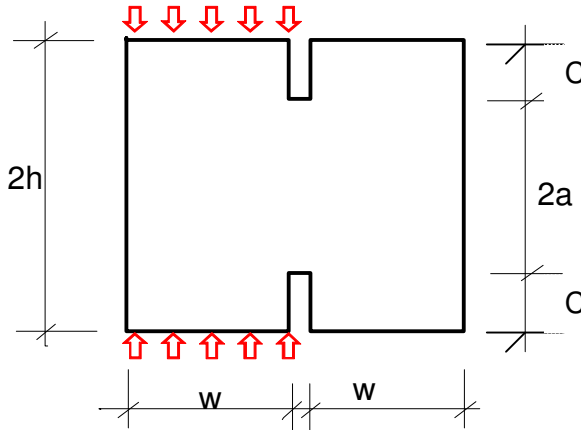

Figure 7. Loading arrangement and specimen configuration used in the numerical study.

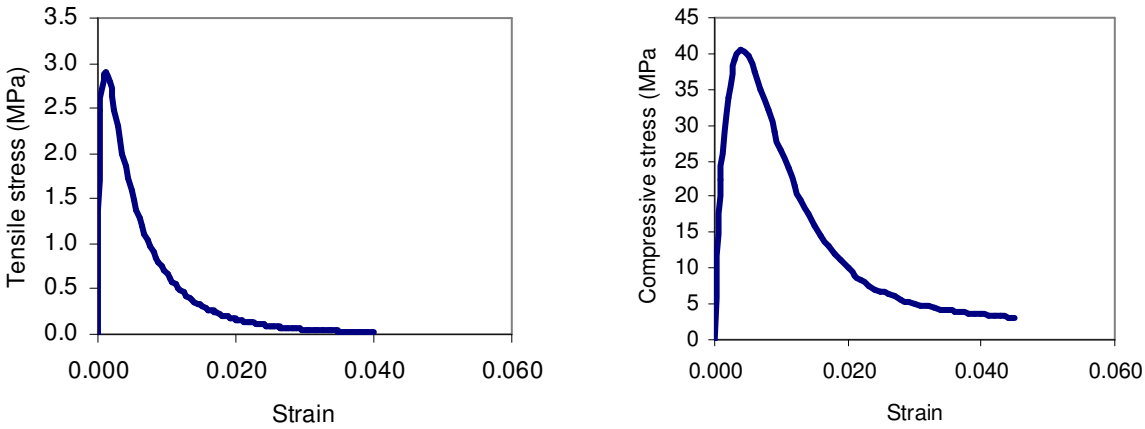

Figure 8. The stress – strain relations assumed in MASA:
(a) uniaxial tension and (b) uniaxial compression.

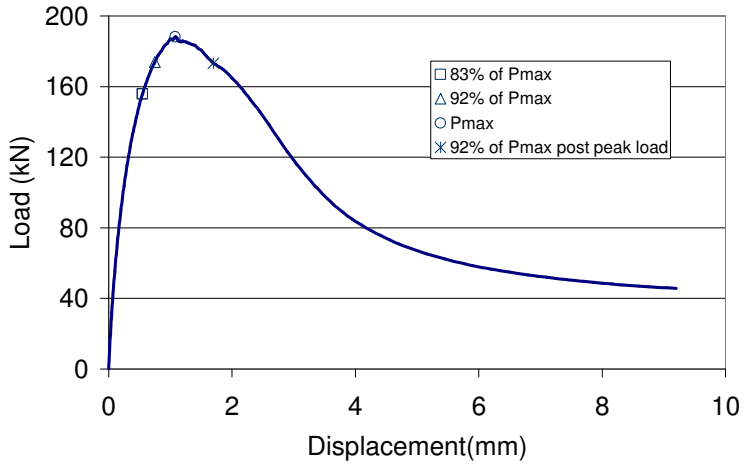

Figure 9. The plot of load vs. displacement gained in numerical study.

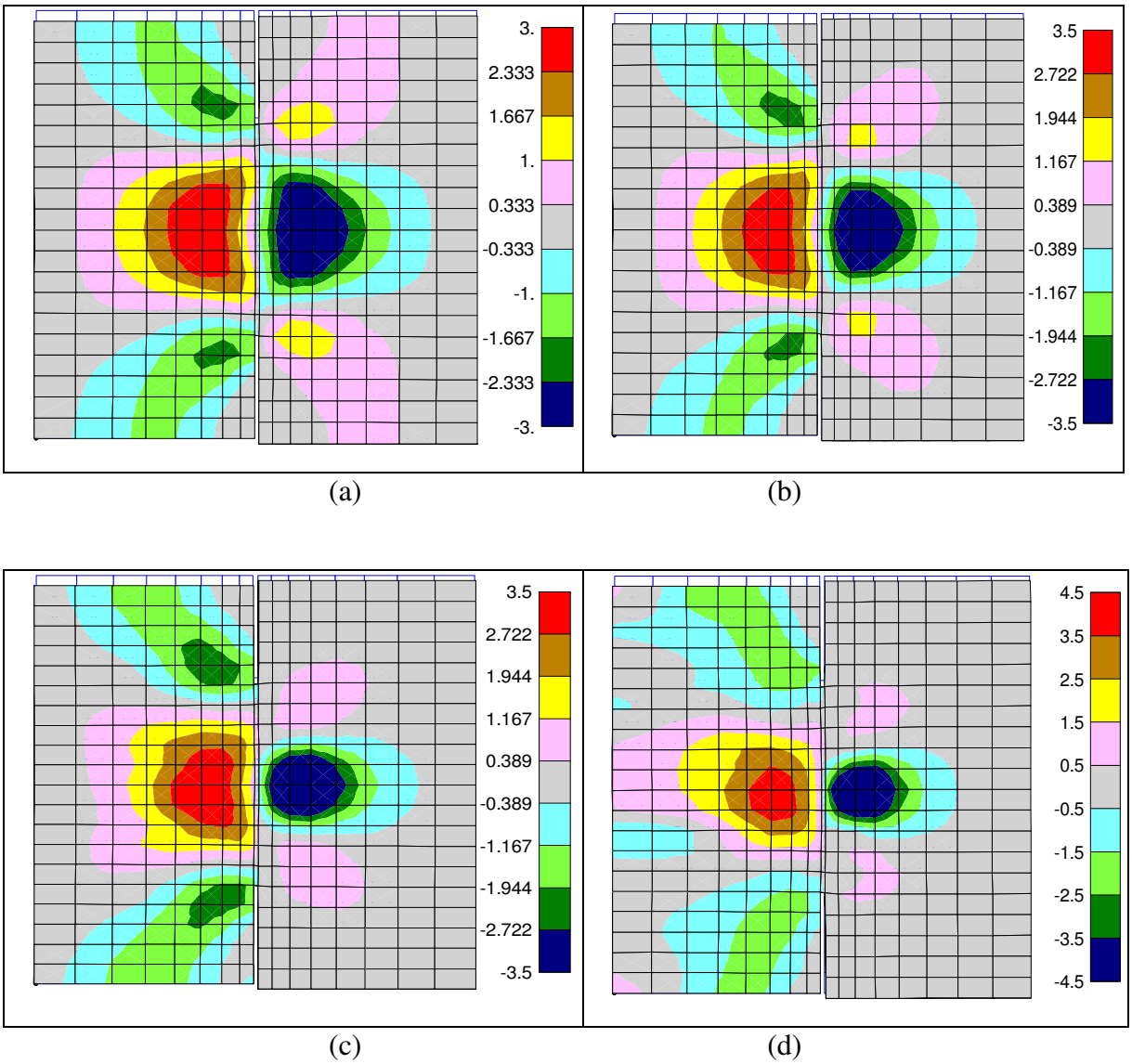

Figure 10. The lateral stresses distributions of four typical loading stages: (a) 83% of P_{max}; (b) 92% of P_{max}; (c) P_{max} and (d) 92% of P_{max} post peak load.

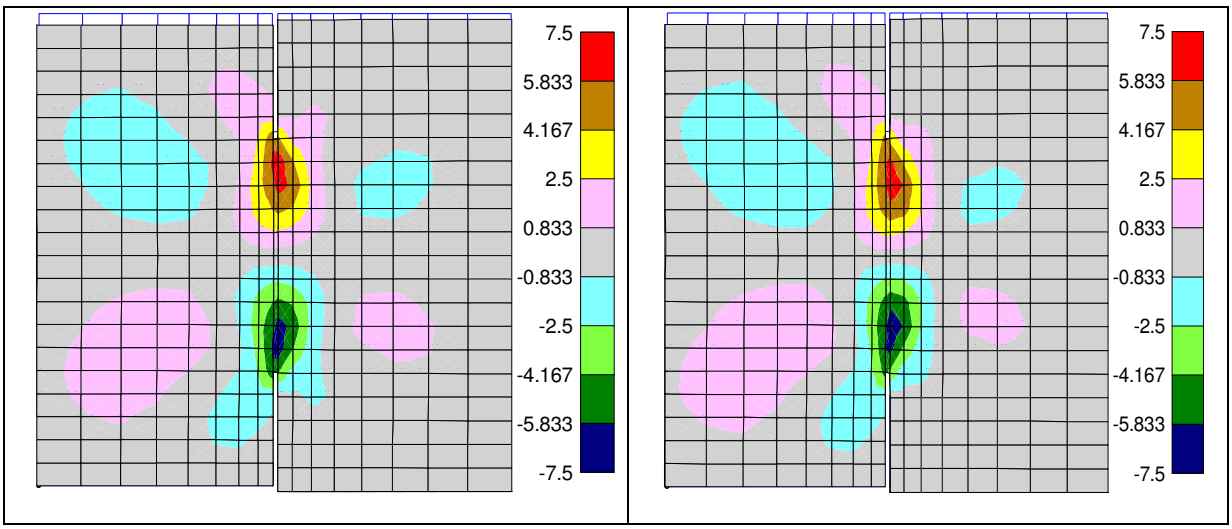

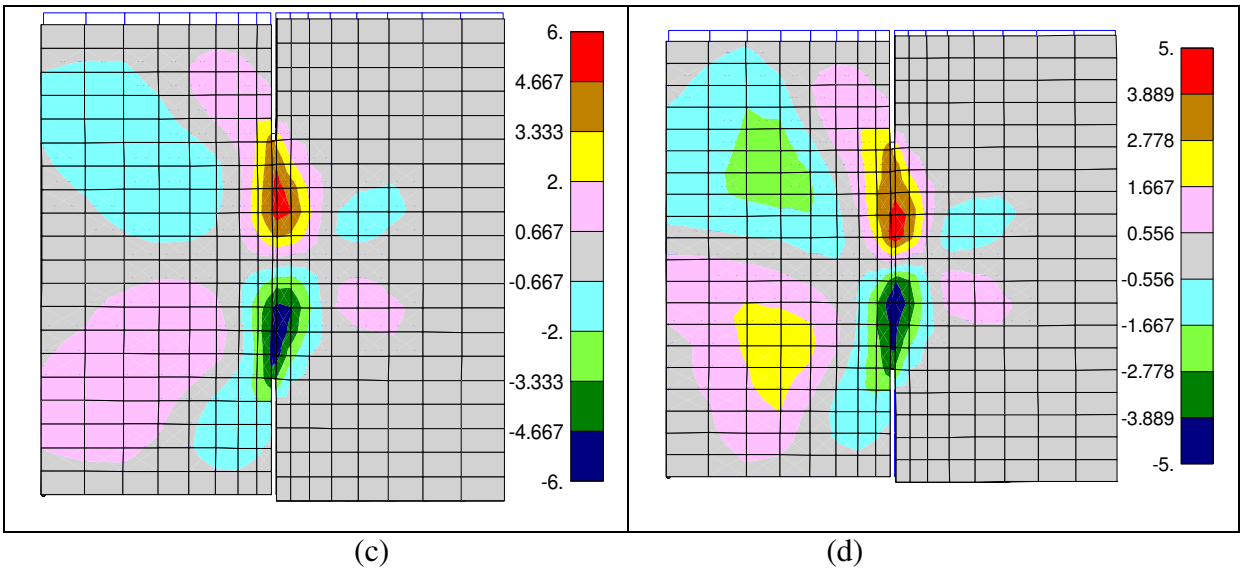

Figure 11. The shear stresses distributions of four typical loading stages: (a) 83% of P_{max}; (b) 92% of P_{max}; (c) P_{max} and (d) 92% of P_{max} post peak load.

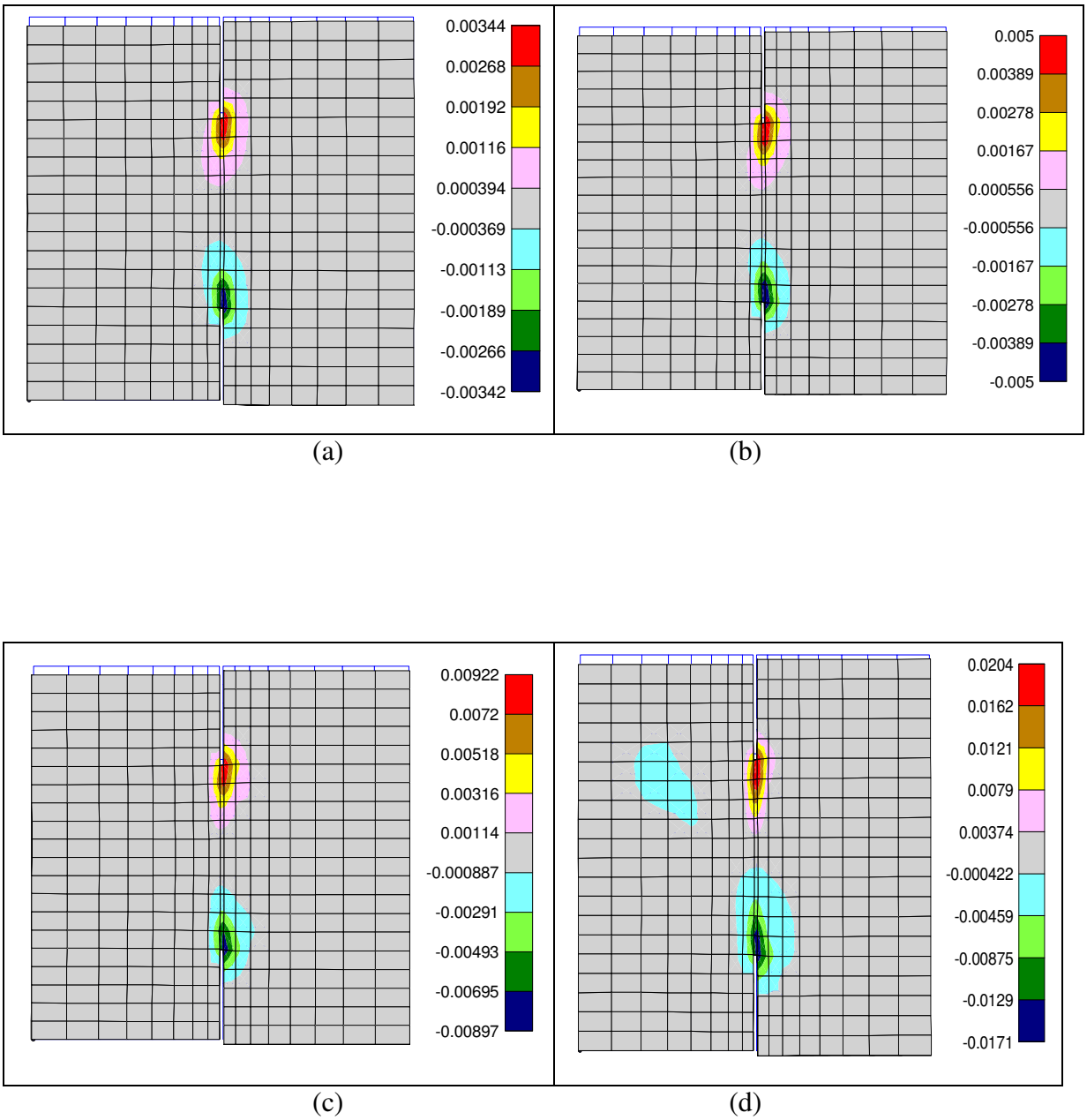

Figure 12. The shear strain distributions of four typical loading stages: (a) 83% of P_{max}; (b) 92% of P_{max}; (c) P_{max} and (d) 92% of P_{max} post peak load.

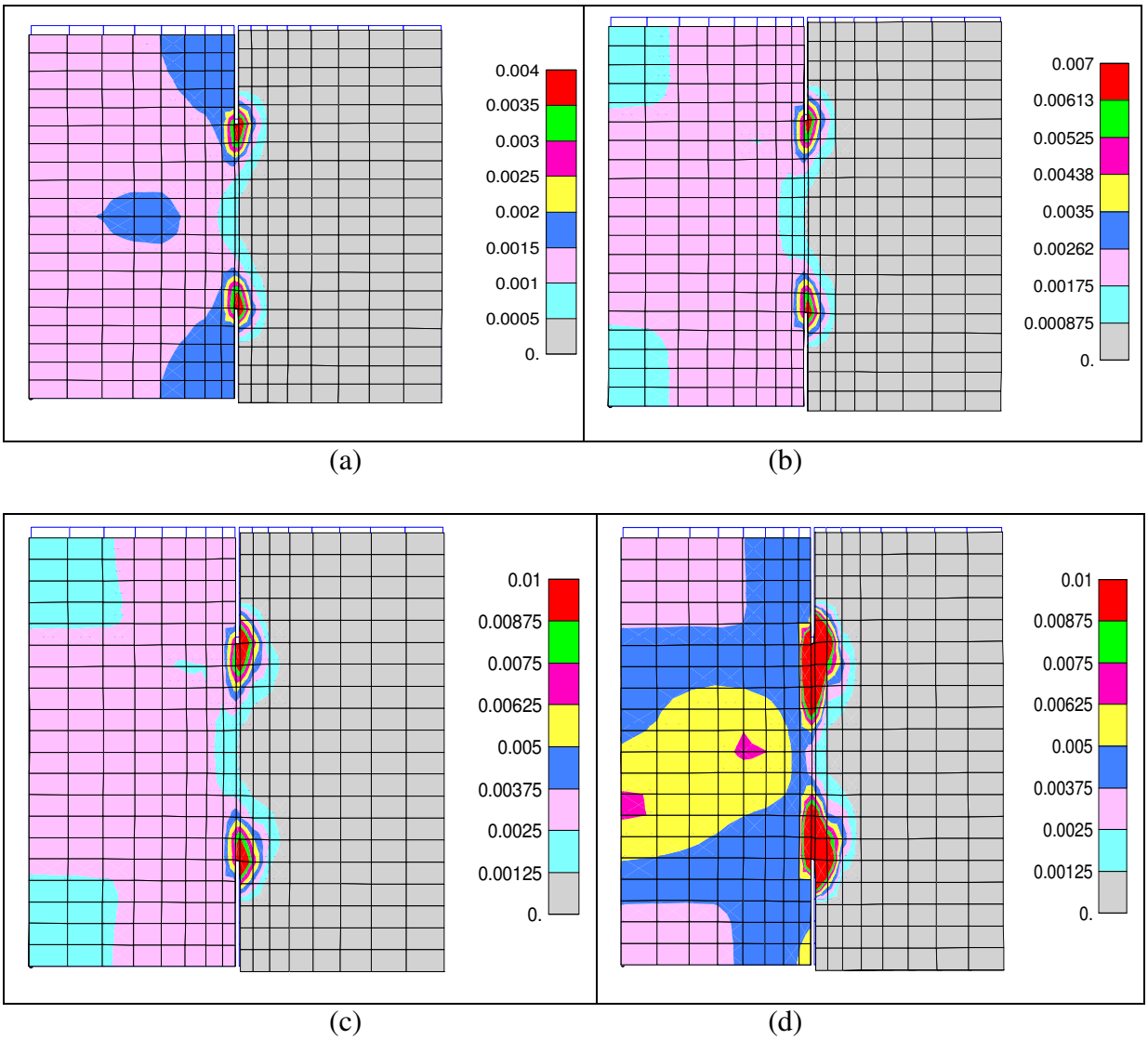

Figure 13. The principle strain distributions of four typical loading stages: (a) 83% of P_{max}; (b) 92% of P_{max}; (c) P_{max} and (d) 92% of P_{max} post peak load.

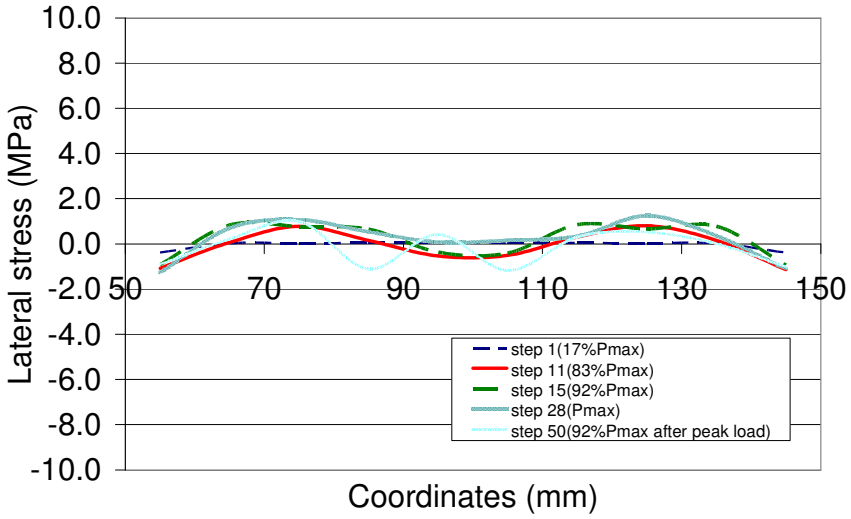

Figure 14. The lateral stress distributions along the ligament at the different loading stages.

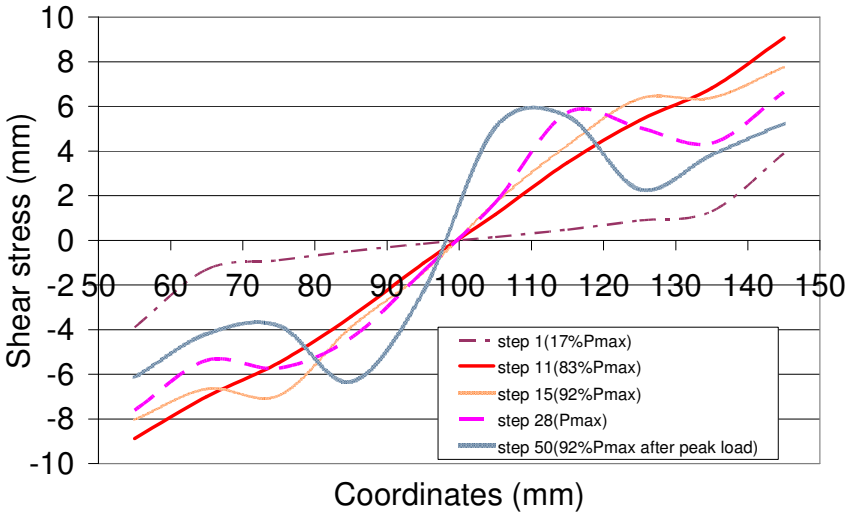

Figure 15. The shear stress distributions along the ligament at the different loading stages.

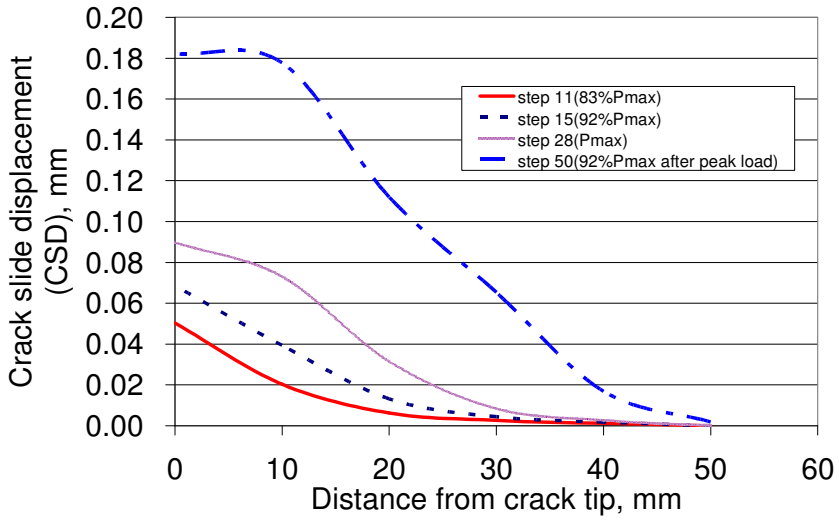

Figure 16. The crack slide displacement along the ligament at the different loading stages.

Especially, the stress distributions along the ligament were studied in detail. The lateral stresses along the ligament for several loading stages are illustrated in Figure 14 and the shear stresses in Figure 15. It can be seen that the tensile or compressive stresses distributed along the ligament that are far lower than the corresponding strength values. It shows that tensile failure cannot happen along the ligament. The shear stress distributions indicate that even though the loading level is lower, the shear stress concentration has already appeared in the front of ligament. With increase of loads, the high shear stresses go forward to centre of the ligament. The highest shear stress level appeared along the ligament when load arrives at 83% of P_{max}, which corresponds about to the critical

shear fracture. It is confirmed once more that the shear fracture along the ligament occurred prior to the compressive failure in the loaded part.

Figure 16 presents the crack slide displacement (CSD) distributed on the ligament. At the tip of the preformed crack, the mode II CSD_c is 0.05 mm corresponding to the critical shear fracture.

4. MODE II TESTS FOR DETERMINING MODE II FRACTURE TOUGHNESS K_{IIC}

In this section, we will introduce the testing method to perform mode II fracture tests for measuring mode II fracture toughness of normal strength concrete (see [38] in details) . It includes the specimen preparation, specimen sizes, loading arrangement, testing procedure, data recording, distinguishing of the critical shear fracture state and the calculation of mode II fracture toughness K_{IIc}.

4.1 Specimen preparation

According to the requirements shown in equations (1) and (6), the height of the specimen should meet condition of $h \geq 2a$ for a uniform stress distribution on the two end of the loaded specimen. The width of specimen mainly depends on the strength of the materials tested for having a satisfied ratio of σ_c / σ_{max}. The lower the value the better because it means that the shear crack develops far before the loaded part of the specimen fails under compression. To reach this, the initial notch should not be too shallow. From the experience of this investigation the notch depth should be 20 to 50 mm if the depth of the specimen is 200 mm. It turned out that the width of the specimen is important and it should not be too small. To secure good handling, the thickness of the specimen should be 50 mm to 100 mm. Table 1 contains some proposed and expected values for different strength classes of concrete. For convenience to prepare specimens according to different strength classes of concrete, one could referee the specimen sizes shown in Table 1. The notch should be cut out or be cast with a width of 1mm to 4 mm.

Table 1. Proposed and expected critical stress for h = 100 mm and d = 100 mm

Cube strength, MPa	25	35	45	65	85	105
Assumed K_{IIc}, MPa $m^{1/2}$	1.7	1.9	2.2	3.3	4.4	5.5
Proposed half width w, mm	200	200	200	100	100	100
Expected critical stress, MPa	15	17	20	42	56	70

It follows from Table 1 that a 200 mm cube could be cut into two halves if high strength concrete is to be tested. Lower grade concrete needs larger specimens because the material is less brittle. The weight of such a specimen is the same as a 200 mm cube.

4.2 Testing procedure

The tests of the double-edge notched plate specimens (DENP) should be carried out in a compressive testing machine being of enough stiffness with closed-loop servo control. The specimen is grounded to make the two loading surfaces smooth and parallel to each other. Steel plates with smooth surface were put under and on top of one half of the specimen. For eliminating friction between steel plate and concrete, a sheet of PTFE has to be added at either side. Finally, the whole arrangement consisting of steel plates and specimen was positioned very carefully between the loading platens of the testing machine in order to avoid eccentricity. The testing arrangement configuration is illustrated in Figure 17. The load should be applied with constant cross-head displacement rate of 0.002 mm/s to 0.006 mm/s at the beginning and of 0.001 mm/s to of 0.003 mm/s when about half of the expected maximum load was reached.

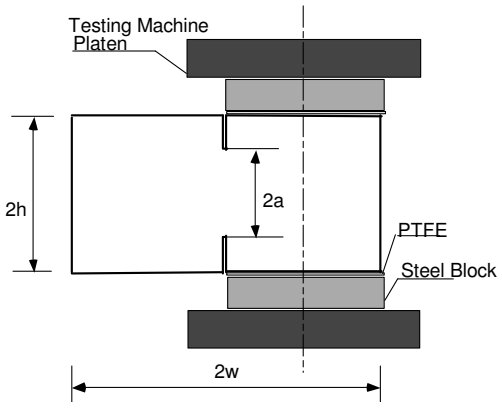

Figure 17. Testing arrangement for normal concrete

During testing, the following displacement should be continuously recorded using LVDTs: the total displacement between the loading platens, the shortening of the specimen on both surfaces of the loaded part on a distance of the height of the specimen and the notch tip opening (here called crack tip opening displacement, *CTOD*). The measuring signals should be digitized, amplified and stored using a computer data collection system.

Eq. (1) predicts for a constant K_{IIc} that the critical stress is

$$\sigma_c = \frac{4 K_{IIc}}{(\pi a)^{1/2}} \tag{7}$$

This means that σ_c is smallest at the beginning of the test and σ_c increases when a crack is initiated at the notch tip and is propagating. Therefore, it is expected that the load vs. displacement shows a discontinuity when a crack is generated.

4.3 Observation on crack pattern in mode II fracture tests

The results gained in numerical study showed that using the geometry configuration and the loading arrangement the shear stress concentration occurs at the crack tip. It is an expectation that mode II crack will propagate along the ligament within a certain range in front of the notch tip. We must also note such a fact that due to the compressive loading acted on the half part of the specimen, the compressive failure (lateral tensile failure) must happed in the loaded part of the specimen after the compressive strength is exceeded. When the height of the tested specimen is too large, it could lead to a tensile failure happened in the unloaded part of the specimens. This means that after the final failure happened in the whole specimen, one can find different types of failure in different parts in the specimens. Regard to that the ligament own is a part of the outline of the loaded part, the shear crack could be perhaps misinterpreted as one among the distributed cracks at the loaded part. Therefore, it is important that one must carefully chose the correct specimen size according to the strength of the tested material and exactly perform the mode II fracture tests to ensure that the shear fracture firstly occurs prior to the compressive failure happened in the loaded part caused by the maximum load. Herewith, several typical shear crack patters observed in mode II fracture tests are described for having basically an understanding the shear crack.

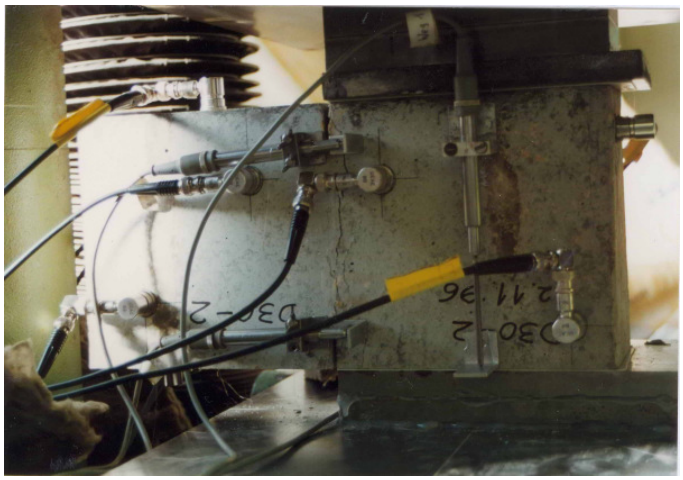

Figure 18. The shear crack initiates at the tip of bottom notch that was observed in test on specimen D30-2 (after test).

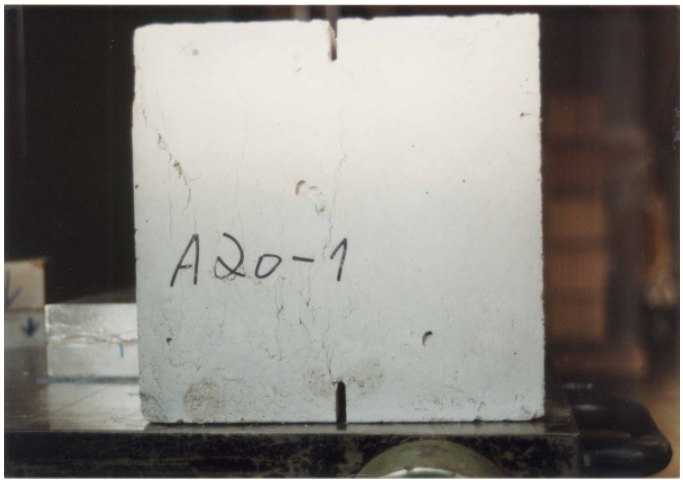

Figure 19. Crack pattern of a specimen from series A with 20 mm notch depth

Figure 20. Crack pattern of two specimens from series D with 30 and 40 mm deep notches

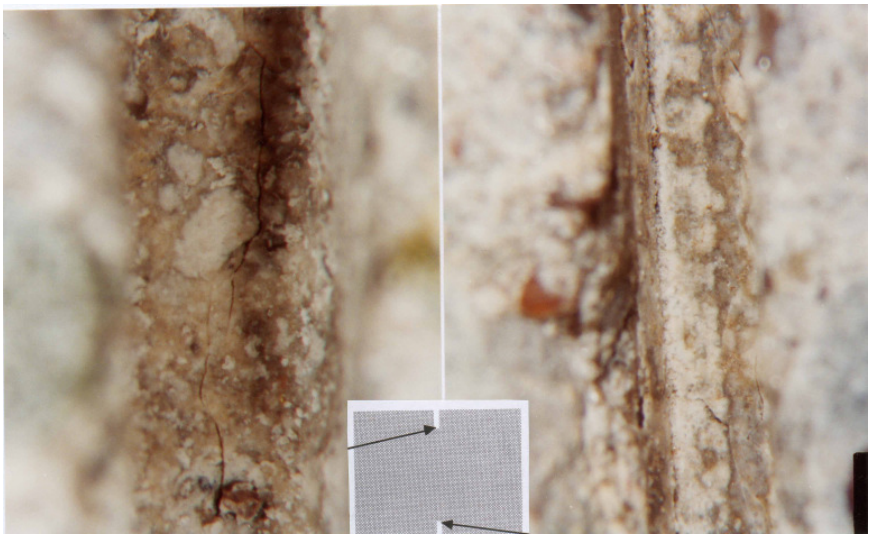

(a) (b)

Figure 21. The microphotographs of shear crack in specimen D20-2; (a) taken at the bottom of the top notch; (b) taken at the bottom of the bottom notch.

During tests, the surface of the specimens especially the area around the notch should be carefully observed. At a certain loading a shear crack initiated at the tip of the notch. Sometimes, the crack propagated along the ligament, sometimes these were inclined cracks in the loaded part of the specimen. There was not a great difference between the load which caused shear cracking and the one causing compression failure which will be discussed later. Figure 18 shows the shear crack initiated from the tip of bottom notch. Differently, on the upper part, the shear crack begun from the top notch tip is merged into the cracks in the loaded part. Figure 19 shows another example where the shear crack started at the notch tip and merged into distributed cracks at the loaded part. Figure 20 shows a different example where the crack started from both notch tips and propagated towards the middle of the ligament to coalesce. These last examples concern tests which were stable during crack initiation and further rapid crack propagation.

By a way, we would like to describe the observation in the test on specimen numbered D30-1. In the test on specimen D30-1, after shear fracture happened along the ligament, no cracking occurs in the loading part of the specimen. Then, the loading stops. The specimen was taken out to observe carefully whether there is some cracking in the loaded part of the specimen. The observing result shows that no any cracking is found in the loading part of the specimen. After observation, the specimen D30-1 was replaced and reloaded until

failure. Now, the cracks in the loaded part of the specimen as seen in the photograph were generated during the second reloading.

Figures 21 shows the microphotographs of shear crack taken at the top and the bottom notches of specimen D20-2. After the test, no body finds any shear crack on the surfaces of the specimens. But, during the test, the discontinuity appeared on the recorded plot of load versus displacement implied that the shear crack started already at the tip of the notches. Therefore, the microphotographs were taken and the shear crack occurred at the both notches were observed. It provides a good proof to the predication using Equation 7.

4.4 Distinction of critical shear fracture load

Now, we would like to introduce how to distinguish the critical shear fracture state using the discontinuity shown on the plots of load vs. displacement. Here, four plots of load vs. displacement are selected which are typical as examples. Figure 22 shows a plot of load vs. displacement between loading platens. Due to the strain of the PTFE layer there is a nonlinear relation mainly in the beginning.

A pronounced discontinuity appears at about 176 kN due to crack initiation. After some load release the load increases again up to the maximum load which causes final compression fracture in the loaded part. When the PTFE deformation is subtracted from total displacement the load vs. displacement relation becomes almost linear up the point of discontinuity. A similar corrected plot is given for specimen B30-1, C30-1 and D30-1 in Figures 23, 24 and 25.

All figures contain the point of discontinuity which will be used later for the computation of the critical stress and hence K_{IIc}. It should be mentioned that the line for D30-1 is not complete and does not show the maximum load. Because the plots for load vs. displacement measured on the surface of the specimen is almost the same as the figures above they are not shown.

The plots of load vs. displacement are typically almost linear up to the point of discontinuity that is identified as the critical point of mode II fracture. As concrete is not really a brittle material, prior to the critical point, a small region of the line is slightly nonlinear. Therefore, the two formulae which are given in the equations (1) and (6) and which are developed from linear elastic fracture mechanics can be approximately applied to the critical fracture load.

For concrete materials, the compressive loading arrangement is illustrated in Figure 17. After the PTFE deformation is subtracted from the total displacement that was measured between the loading platens, the typical plots of the load vs. corrected displacement are shown in Figure 22 to Figure 25 for four different concrete mixtures. The line for specimen D30-1 is not complete and the maximum load is not shown in Figure 25. All plots show significant discontinuity mark. The relation up the point of discontinuity is almost linear.

According to the specimen sizes tested in the experiments, the critical mode II stress intensity factors for several concrete materials were determined submitting the critical fracture stress σ_c into formulae (1) and (6). It was shown that the ratio of the critical fracture stress σ_c to the maximum stress σ_{max} which corresponds with compressive failure of the loaded part of a tested specimen, depends on both the half width w of the specimen and the concrete strength.

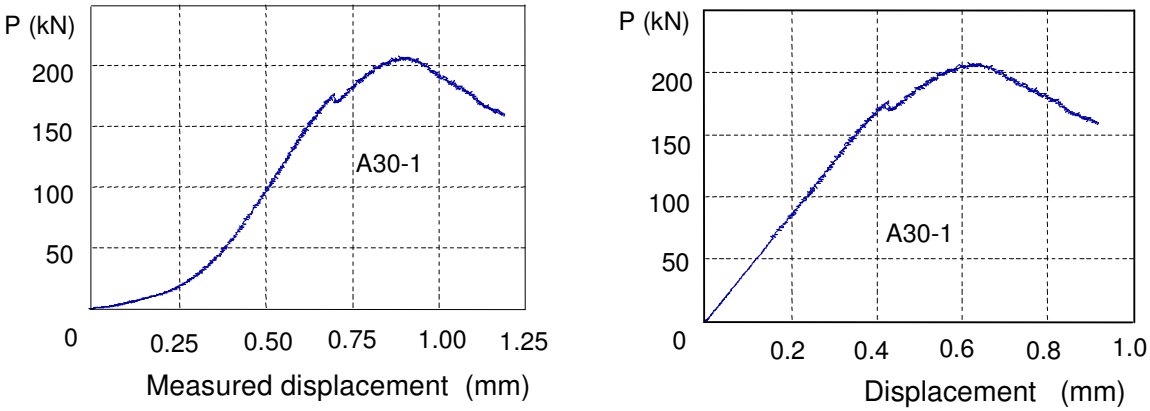

Figure 22. Load vs. displacement between loading platens of specimen A30-1; a) direct measurement; b) corrected.

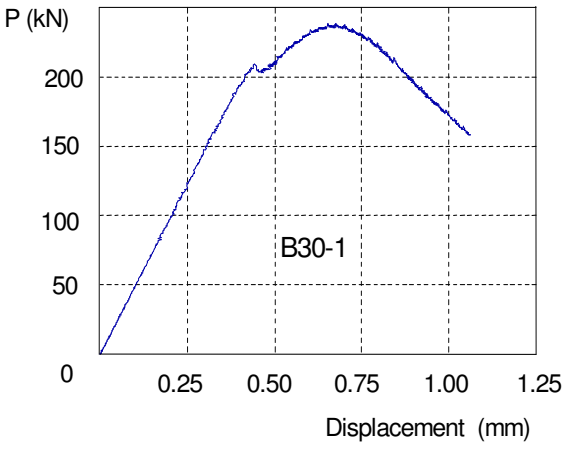

Figure 23. Load vs. corrected displacement for specimen B30-1.

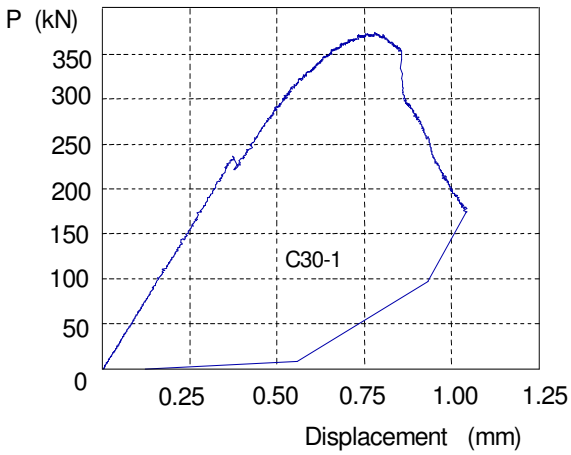

Figure 24. Load vs. corrected displacement for specimen C30-1.

Careful observation for all measured plots was made. It had been found that for a same specimen the points of discontinuity on the plots of load vs. total displacement, load vs. deformation and load vs. *CTOD* almost corresponds the same load value. According to the investigation to the tests on the specimens of series D, it is known that the point of discontinuity on the measured plots is caused by critical fracture of the preformed cracks in the tested specimens.

In order to determine whether the points of discontinuity on the plots measured from other testing series A, B and C are caused by the critical cracking of the preformed cracks too, further comparison should be made. As a comparing test, a curve of load versus total displacement between two platens of the testing machine and a curve of load versus deformation were measured on a cube specimen with side length of 200 mm, without preformed notches. The test for the cube was under a same testing condition. The layer of Teflon was put too for keeping the boundary condition as the same as the shear fracture tests, reducing friction between the surfaces of steel block and concrete. The measured plots of load versus total displacement of the cube numbered DC-1 are given in the Figure 26.

It can be seen that there is no any observable discontinuity on the ascending branches of the plots of the load versus displacement measured from the test on the cube specimen with side length of 200 mm without preformed notches. It is well known that in the compressive tests for concrete when the applied load exceeds about 50% of its maximum load, the observable cracking has already appeared, then, will continually develop until final collapse. The testing result of the cube specimen without preformed notches, as evidence on another aspect, confirms that the point of discontinuity on the plots of the load vs. displacement measured from the shear fracture tests on the double-edge notched plate specimens can solely be caused by the critical shear fracture of the preformed cracks in the specimens.

According to the characters appeared in the all curves from Figure 22 to Figure 26 and the investigation to the tests on specimens of series D, it can be confirmed that the point of discontinuity on the plots of load versus displacement is a critical shear fracture point. The corresponding load must the critical shear fracture load P_c. Therefore, the critical stress intensity factor of mode II, K_{IIc}, can be determined using the critical shear fracture load P_c.

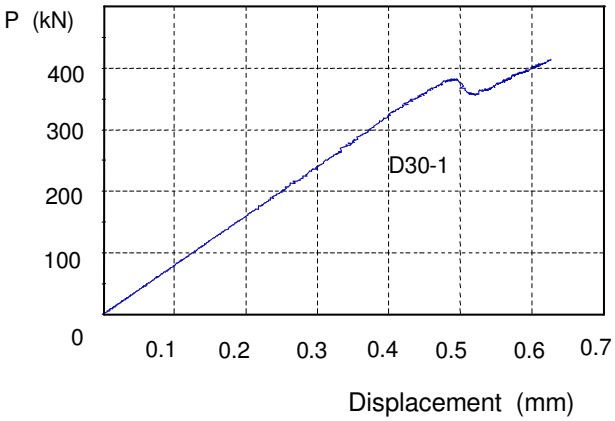

Figure 25. Load vs. corrected displacement for specimen D30-1.

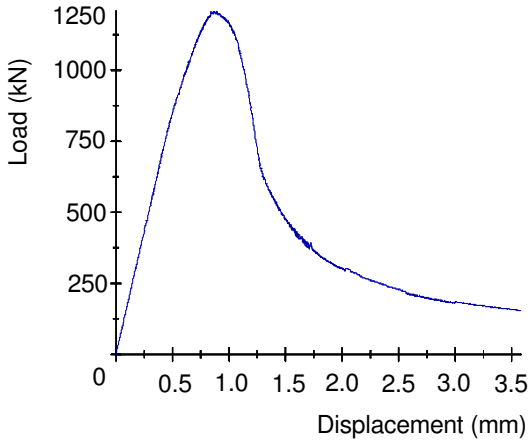

Figure 26. Load vs. corrected displacement for cube specimen DC-1.

4.5 Experimental determination of K_{IIc} values

After the appearance of the cracks and the typical load-displacement behaviour were understood it seemed acceptable to calculate the fracture toughness K_{IIc} from the stress at the discontinuity point. Table 2 summarizes the results of all specimens tested.

Using the testing data gained in our mode II fracture tests shown in Table 2, the procedure for determining mode II fracture toughness K_{IIc} is introduces in details as follows.

From the column of dimensions, it appears that the real values differ a little from the design value due to the width of the saw blade. Series A and B contain also two specimens with grooves (indicated by k). Critical stress σ_c and maximum stress σ_{max} are supposed to be uniform over the cross-section. Eq. (6) is used for calculating K_{IIc} although, strictly, the condition of $h \geq 2a$ is only met in four cases. However, the more important condition $w \leq \pi a$ is met in all cases.

Meanvalues, standard deviation (S.D.), and coefficient of variation (C.V.) is given for the four series. The rounded mean values of K_{IIc} are 1.68, 1.86, 2.00 and 2.04 MPa $m^{1/2}$, the respective coefficients of variations are 7.2, 10.7, 8.8, and 6.9%. These values are not larger than usual variations of mechanical properties of concrete. The K_{IIc} values are higher than about twice K_{Ic} values obtained by other researchers.

Table 2. Testing results of all specimens

Specimens	Dimensions *wxhxd(d_n)* (mm)	Half Length of ligament *a* (mm)	P_c (kN)	P_{max} (kN)	σ_c *(MPa)*	σ_{max} (MPa)	K_{IIc} (MPa $m^{1/2}$)	σ_c/σ_{max}
A10-1	97.8x100x 93.7	90	211.5	211.5	23.08	23.08	1.804	1.000
A10-2	98.0x100x99.0	90	207.0	220.0	21.34	22.68	1.670	0.941
A20-1	97.8x100x93.9	80	204.7	223.0	22.29	24.28	1.743	0.918
A30-1	98.5x100x93.1	70	176.0	206.3	19.21	22.51	1.507	0.853
A30-2	97.8x100x99.5	70	178.2	235.0	18.31	24.15	1.432	0.758
A40-1	97.7x100x92.4	60	185.5	197.8	20.56	21.92	1.606	0.938
A40-2	97.5x100x99.4	60	222.2	226.0	22.93	23.32	1.790	0.983
A40k-1*	98.6x100x96.7(39.4)	58.3	158.0	213.0	16.59*	22.34	1.757	0.743*
A40k-2*	96.6x100x95.7(44.1)	58.4	144.3	202.6	15.58*	21.91	1.670	0.711*
A50-1	98.9x100x98.8	50	215.9	215.9	22.09	22.09	1.737	1.000
A50-2	96.9x100x93.5	50	205.0	205.0	22.63	22.63	1.767	1.000
Mean					21.38	22.81	1.682	0.933
S.D.					1.695	0.823	0.122	0.082
C.V.					0.079	0.036	0.072	0.087
B10-1	98.3x100x97.9	90	170.0	258.5	17.67	26.89	1.385	0.657
B10-2	96.4x100x94.1	90	no	278.6	no	30.72	no	no
B20-1	97.9x100x93.5	80	229.3	240.0	25.05	26.22	1.959	0.955
B20-2	98.5x100x97.7	80	212.8	276.2	22.11	28.71	1.735	0.770
B30-1	99.1x100x93.4	70	207.8	238.0	22.45	25.72	1.767	0.873
B30-2	98.3x100x98.6	70	210.3	263.2	21.7	27.16	1.701	0.799
B40-1	99.9x100x93.2	60	237.0	243.0	25.45	26.10	2.010	0.975
B40-2	98.5x100x98.2	60	238.0	259.1	24.6	26.78	1.931	0.919
B40k-1*	98.4x100x97.0(38.6)	59.5	180.4	282.6	18.90*	29.60	2.042	0.639*
B40k-2*	98.8x100x95.7(37.1)	59.1	175.0	264.4	18.51*	27.97	1.994	0.662*
B50-1	99.3x100x95.2	50	237.8	237.8	25.16	25.16	1.982	1.000
B50-2	98.5x100x96.4	50	242.4	253.1	25.53	26.66	2.003	0.958
Mean					23.30	27.31	1.864	0.878
S.D.					2.603	1.651	0.200	0.115
C.V.					0.112	0.060	0.107	0.130
C20-1	97.1x100x99.2	80	225.0	331.5	23.40	34.4	1.821	0.680
C20-2	98.1x100x96.3	80	280.0	417.0	29.64	44.14	2.321	0.671
C20-3	98.0x100x99.6	80	255.0	355.6	26.12	36.43	2.045	0.716
C20-4	97.1x100x98.3	80	232.8	351.0	24.39	36.78	1.900	0.663
C30-1	98.4x100x98.4	70	236.0	374.0	24.37	38.63	1.911	0.631
C30-2	97.2x100x99.3	70	246.0	382.0	25.50	39.60	1.987	0.644
Mean					25.57	38.33	1.998	0.668
S.D.					2.210	3.374	0.176	0.030
C.V.					0.086	0.088	0.088	0.045
D20-1	200.4x100x101.0	80	397.8	559.0	19.65	27.62	2.199	0.711
D30-1	197.4x100x102.4	70	380.0	490.0	18.80	24.24	2.090	0.776
D30-2	199.5x100x100.9	70	359.4	530.0	17.85	26.33	1.993	0.678
D40-1	199.0x100x102.9	61	351.0	495.0	17.10	24.17	1.871	0.707
Mean					18.35	25.59	2.038	0.718
S.D.					1.111	1.684	0.140	0.041
C.V.					0.061	0.066	0.069	0.058

** The values are not included in the calculation for the values of mean, S.D. and CV.*

For the four specimens numbered A40k-1, A40k-2, B40k-1 and B40k-2 in the Table 2, two kerfs with the width of 4 mm were sawn on the both lateral sides along the ligament for each one. In the calculation for K_{IIC}, the conventional assumption of section equivalence was used as the same as in [32]. The thin thickness b_n of the ligament are given in the corresponding parentheses in the Table 2. However, due to inhomogeneity of concrete, complete shear fracture exactly along the ligament cannot always happen. Besides the drawback that the cracking process along the ligament cannot be directly observed, the critical shear fracture point on the recorded plots of load versus displacement is less observable than in the tests on wood and its distinction is not so easy. A great care must be taken for distinguishing it. So, it is unsuitable for concrete mode II tests to make two kerfs on both lateral sides along the ligament.

In the test on the specimen numbered B10-2, no any shear cracking was found. On the recorded plots of load versus displacement and other plots, no any observable discontinuity can be found too. So, the corresponding result for K_{IIc} was lack in the Table 2.

Figures 22 to 25 indicate that there is some stable crack development prior to the critical load and also between critical and maximum load. This means that fracture energy is dissipated and a G_{IIF} value would apply. A practical approach to determine mode II fracture energy G_{IIF} will be introduced in next section.

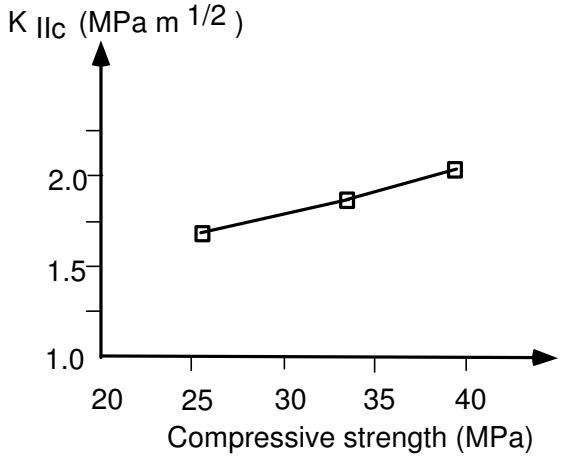

Figure 27. K_{IIc} *vs.* $f_{c,cube}$

A plot of K_{IIc} vs. $f_{c,cube}$ of series *A, B, D* shows a relation which increases with strength (see Figure 27). Series *C* is omitted because the composition of the concrete is not known. Despite the little amount of data this relation is not in

contradiction to other fracture mechanics parameter dependencies on compressive strength.

5. DETERMINATION OF MODE II FRACTURE ENERGY G_{IIF} OF CONCRETE USING A PRACTICAL APPROACH

As well known, in the mode I fracture tests, for example, when an extra load is applied to a three-point bending notched beam, the beam can be completely separated two parts and the extra work could be assumed to be wholly dissipated by the fracture process zone along the whole ligament. Differently from the mode I test on beam, in mode II fracture test on double-edge notched specimen, the extra work is not only dissipated by the shear crack propagation along the ligament, but also by compressive failure happened in the loaded part and tensile failure in the unloaded part. In order to evaluate the mode II fracture energy, our main attention will focus on the energy to drive the crack propagation near the notch tip. However, it is very difficult to determine directly the mode II fracture energy. Reinhardt and Xu (2000)[39] proposed a practical approach to evaluate the mode II fracture energy of concrete. In this section, we introduce this approach as follows in details.

5.1 Basic consideration and specimen preparation

The idea to measure G_{IIF} is to compare the load vs. displacement plots of double-edge notched specimens with different ligament lengths. The difference between such lines is due to the extra work which is dissipated by mode II displacement. The longer ligament the larger the extra work. This extra work is considered to be mode II fracture energy when the specimen is completely separated along the ligament.

It is well known that concrete is inhomogeneous. The scatter of its mechanical properties is quite considerable. The influence of a small difference of ligament length on a change of the initial compliance of load vs. displacement may be of the same amount as caused by the inhomogeneity. In our previous experiments on the double-edge notched specimens it was found that the difference of the initial compliance of load vs. displacement is so small that it could not be detected when the difference of the ligament lengths used in the experiments was equal to or less than 10 mm. So, the difference of the ligament lengths for different double-edge notched specimens should be large enough that the influence of the inhomogeneity of concrete can be ignored.

Table 3. Specimen dimensions used in mode II fracture tests for measure fracture energy

Specimen	Width, 2w (mm)	Depth, 2h (mm)	Thickness (mm)	Notch depth (mm)
DC30-1	200	200	95.7	29.5
DC30-2	200	200	99.8	31.1
DC0-1	200	200	95.7	0
DC0-2	200	200	96.0	0

In order to enable to perform the tests for obtain the extra work differentce between the two specimens with different notch length, from cubes with the same dimensions of 200 x 200 x 200 mm^3, two kinds of specimens will be prepared, of which, one kind of them has a constant notch length being 30 mm sawn with 4 mm wide, and the other one has no notch. The dimensions of the specimens used in the test are given in Table 3. The cube compressive strength of 28 days is 39.5 MPa.

5.2 Loading arrangement and testing procedure

The loading arrangement of the mode II tests for evaluating mode II fracture energy G_{IIF} is the same as that used for determining mode II fracture toughness K_{IIc} mentioned above. According to our experience, it is not so easy to perform such tests. This could be one of the reasons why some researchers reported that their tests on double-edge notched specimens carried out were mixed mode tests, not mode II tests. In order to enable readers understanding more details of the mode II tests, herewith, we prefer to repeat some procedure for performing the mode II tests.

The loading arrangement of the tests on the double-edge notched specimens is shown in Figure 28 (a), and the one without notches in Figure 28 (b). The tests were carried out in the MFL 3 MN compressive testing machine with closed-loop servocontrol. Steel plates with smooth surfaces were put under and on top of one half of the specimen. To eliminate friction between the steel plate and concrete, a sheet of PTFE was added at either side. The whole arrangement consisting of steel plates and specimen was positioned very carefully between the loading platens of the testing machine in order to avoid eccentricity. The load was applied with a constant crosshead displacement rate of 0.003 mm/s at

the beginning and of 0.0015 mm/s when about half of the expected maximum load was reached.

The following displacements were continuously recorded by LVDTs through the Diadem computation system: the total displacement between the loading plates, the shortening of the ligament on both sides of the notch tips and on both surfaces with a distance of about 140 mm. The LVDT that is attached at the front of the specimen and at the loaded part is noted with LF, and at the unloaded part with UF (see Figure 28). On the back surface, they are denoted with LB and UB respectively. For the specimens that have no notches, shown in Figure 28 (b), the LVDTs were attached at both sides of the centre line.

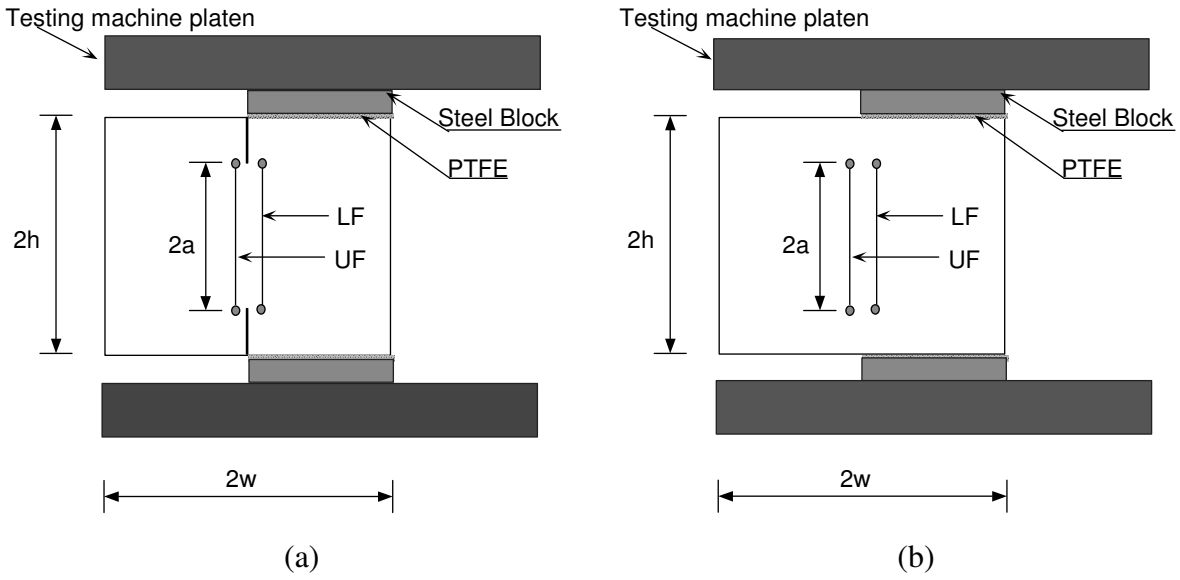

Figure 28. The testing arrangement, (a) the notched specimen; (b) the unnotched specimen.

5.3 Description of observed crack propagation

During the tests, the crack propagation on both kinds of specimens was carefully observed. For the notched specimen, a shear crack started at the tip of the notch when the loading reached a certain value; then, the crack propagated along the ligament; finally, the crack entered the loaded part of the specimen. In the loaded part, vertical cracks could be observed basically parallel each other after the maximum load was reached. The specimens without notches were tested in the same loading arrangement as the one for the notched specimens. Due to the shear stress concentration at the middle points on the bottom and the top of the unnotched specimen, at the edge of the loading steel block, a very shape crack was formed. The two cracks propagated from the bottom and the top

of the specimen and then developed almost exactly along the ligament, e.g., the middle line. Finally, complete fracture occurred along the ligament.

Comparing the observation for the two kinds of specimens, it could be thought that unnotched specimens under the loading arrangement shown in Figure 28 (b) could be more suitable for pure mode II fracture tests. The fact that a very sharp tip of the crack was formed by the shear stress concentration at the edges before crack propagation is very important for mode II fracture. Contrarily, the notches sawn in the notched specimens are 4 mm wide.

How to determine the length of an initial crack formed by the stress concentration needs further study. When the dimension conditions of specimens should satisfy formula (1), one needs to know it for determining K_{IIc}. In fact, the process of an unnotched specimen includes the formation of an initial crack due to the stress concentration and the further propagation of the crack formed.

As a limit case, the length of the initial crack could be assumed to be zero for the unnotched specimen. So the maximum length of the ligament a will be equal to the half depth h of the specimen. Under this condition the stress intensity factor K_{II} will arrive at its maximum value at a certain loading when the formula (1) can be applied. Therefore, the unnotched specimen is most beneficial for initiating fracture.

Although this new problem without notches has to be theoretically solved yet, the new specimen type and the loading arrangement is valuable for carrying out pure mode II tests. Due to the shear stress concentration at the middle point at the bottom and the top of the unnotched specimen, the formation of an initial crack is possible. Then, the sharp tip of a crack is a suitable starter for crack propagation. Finally, the important testing phenomenon is that complete fracture happened along the ligament.

5.4 Distinction of critical shear fracture using the discontinuity shown on the recorded plots of load vs. displacement

The measured displacement between the loading plates, the total displacement includes the deformation of the PTFE layer. Due to the PTFE, there is a nonlinear relation mainly in the beginning (see Figure 22(a)). When the PTFE deformation is subtracted from total displacement, the load vs. corrected displacement for the four tested specimens are given in Figure 29 to Figure 30 for the notched specimens and the unnotched specimens respectively.

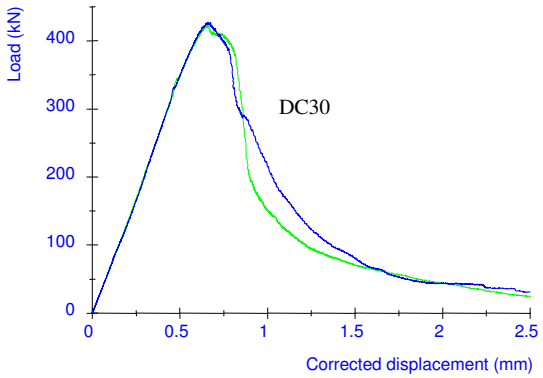

Figure 29. Load vs. corrected displacement for the notched specimens DC30-1 and DC30-2 with 30 mm notch depth.

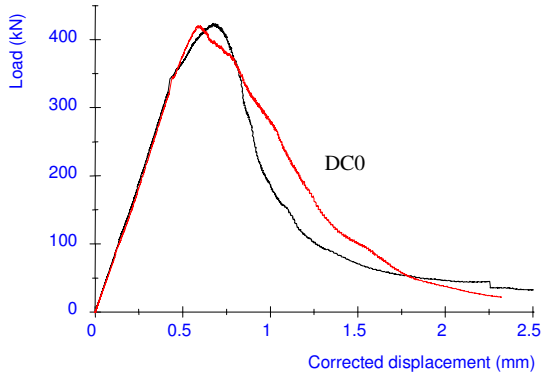

Figure 30. Load vs. corrected displacement for the unnotched specimens DC0-1 and DC0-2.

Some feature of the load vs. displacement curves shown in Figure 29 and 30 should be mentioned. Average loading values P_c at the points of discontinuity and the average maximum load P_{max} are 314 kN and 424 kN for the notched specimens and 321 kN and 421 kN for the unnotched specimens respectively. The plots of load vs. displacement are almost linear up to the points of discontinuity. It is the same observation as the description in section 4 in this Chapter. For each group of specimens, the plots of load vs. displacement including the maximum load and the loads at the points of discontinuity coincided very well.

The load vs. displacement plots measured from the two groups of specimens that have different ligament lengths are drawn in one graph as in Figure 31. A partly enlarged graph is given in Figure 32.

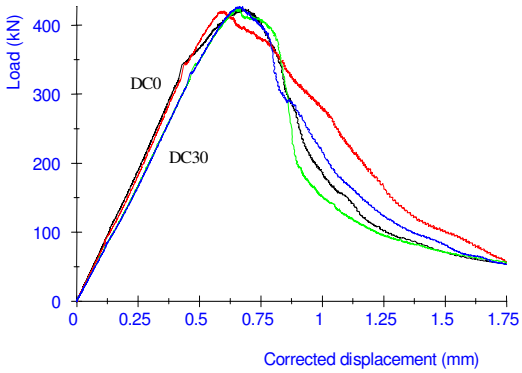

Figure 31. Difference between initial compliance c_i of load vs. displacement due to the difference of ligament length.

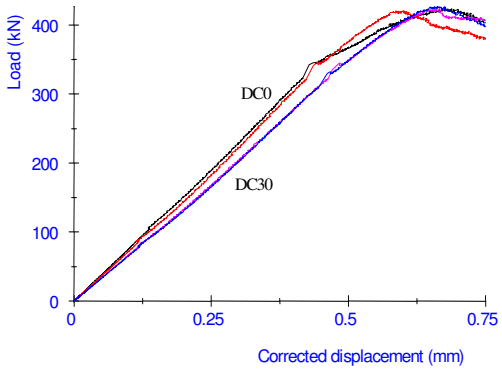

Figure 32. A partly enlarged illustration for the initial compliance difference due to the ligament length.

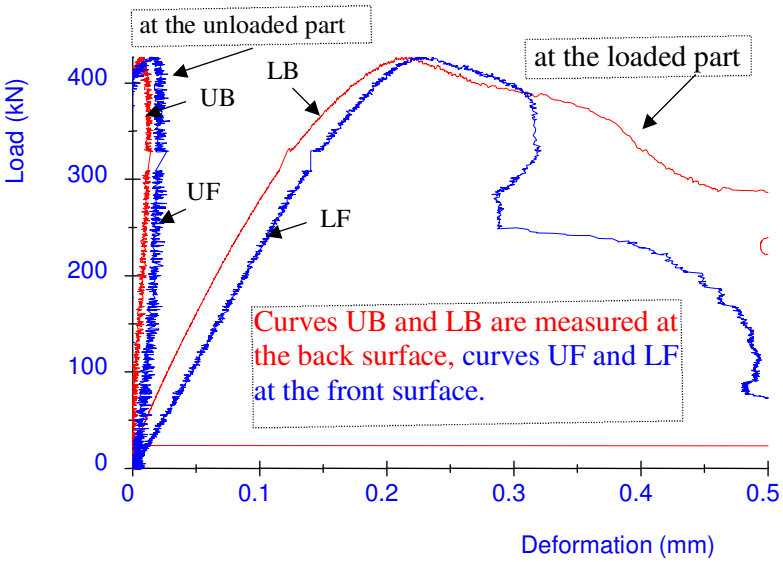

Figure 33. Typical plots of load vs. deformation measured from the back surface and the front at the loaded part and unloaded part (specimen DC30-2).

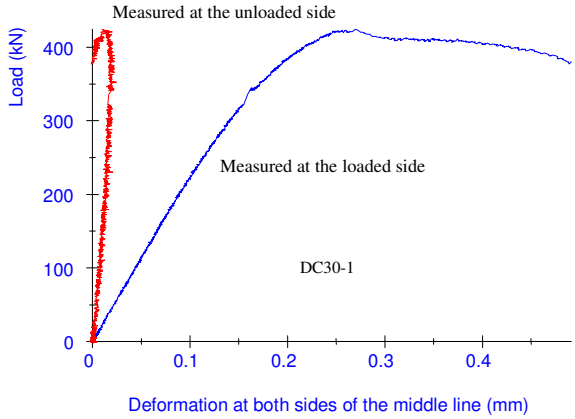

Figure 34. Average plots of load vs. deformation for specimen DC30-1.

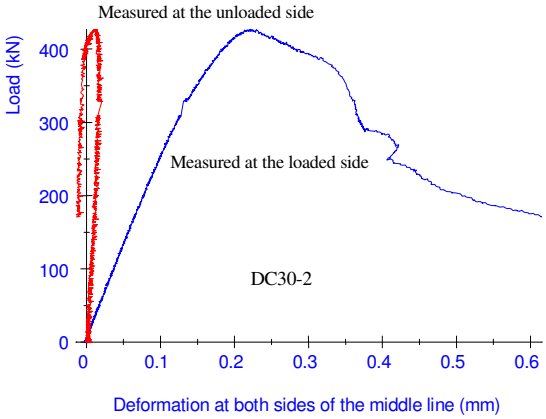

Figure 35. Average plots of load vs. deformation for specimen DC30-2.

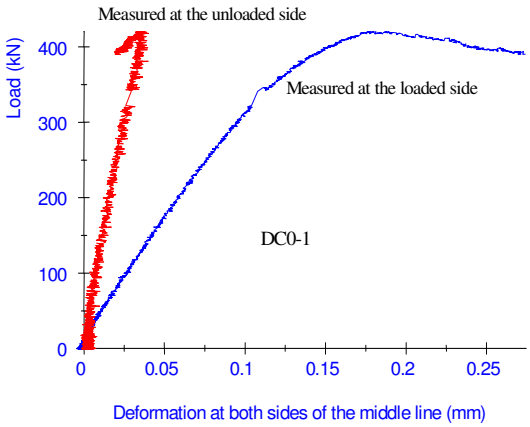

Figure 36. Average plots of load vs. deformation for specimen DC0-1.

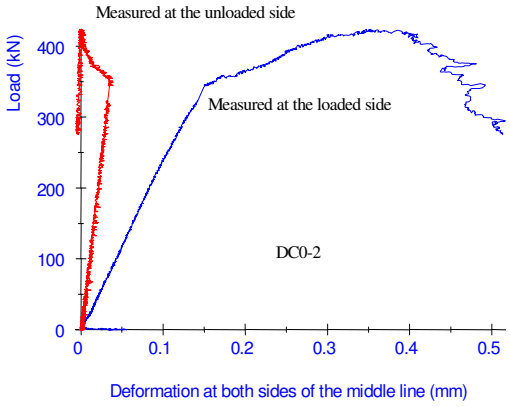

Figure 37. Average plots of load vs. deformation for specimen DC0-2.

Due to enough large difference of ligament length chosen in the tests, the initial compliance difference due to the ligament length are manifested in both the whole relation of load vs. displacement as Figure 31 and the locally enlarged Figure 32. It can be used for the determination of mode II fracture energy. The approach will be introduced in the next section.

In the tests, four LVDTs were used to measure the deformation of the ligament at both sides of the middle line, of which one side is at the loaded part and another one is at the unloaded part, and both the front and the back surfaces of the specimen. The distance to measure deformation is about 140 mm for all specimens. The typical plots of load vs. deformation measured from the frond and the back surfaces are shown in Figure 33. The average plots measured from the two surfaces are given in Figure 34 to Figure 37.

Points of discontinuity can be seen on Figure 34 to 37. They are in agreement with those manifested in plots of load vs. displacement shown in Figure 29 and Figure 30 very well, even though more sensitive than the discontinuous character of Figures 29 and 30. Reinhardt and Xu (1998) [38] attributed the points of discontinuity to the critical point of shear fracture. And Cedolin et al.'s observation (1997) [35] certified that through the moiré interferometry. However, to detect the critical point on the curves of load vs. deformation measured by Cedolin et al. is not easy because the measuring extensometers were positioned far from the local fracture zone [35].

The messages that a plot of load vs. deformation measured from the unloaded part provides are most important for manifesting a shear fracture proc-

ess in the tests. Figure 34 to Figure 37, besides Figure 36, show that the deformation of the unloaded part almost linearly increased until the critical load was achieved. Between the critical load and the maximum load, the deformation slowly decreased due to the shear crack initiation and the propagation. When the loading arrived at the maximum load value, the deformation suddenly went down in the opposite direction. The phenomena imply that after the maximum load was exceeded, the unloaded part can be approximately thought to be free of the action of the loaded part. This means that a part of the total deformation energy was dissipated by the shear fracture along the ligament during the stable crack propagation prior to the critical load and between the critical load and the maximum load. Therefore, it is possible to determine fracture energy in mode II through experiments.

5.5 Determination of mode II fracture energy G_{IIF} of concrete

When experiments are carried out on the two different specimens according to Figure 38 (a) and (b), the initial compliance of load vs. displacement relations was found to be different due to the difference of ligament length. The testing results could be seen in Figure 31 and 32.

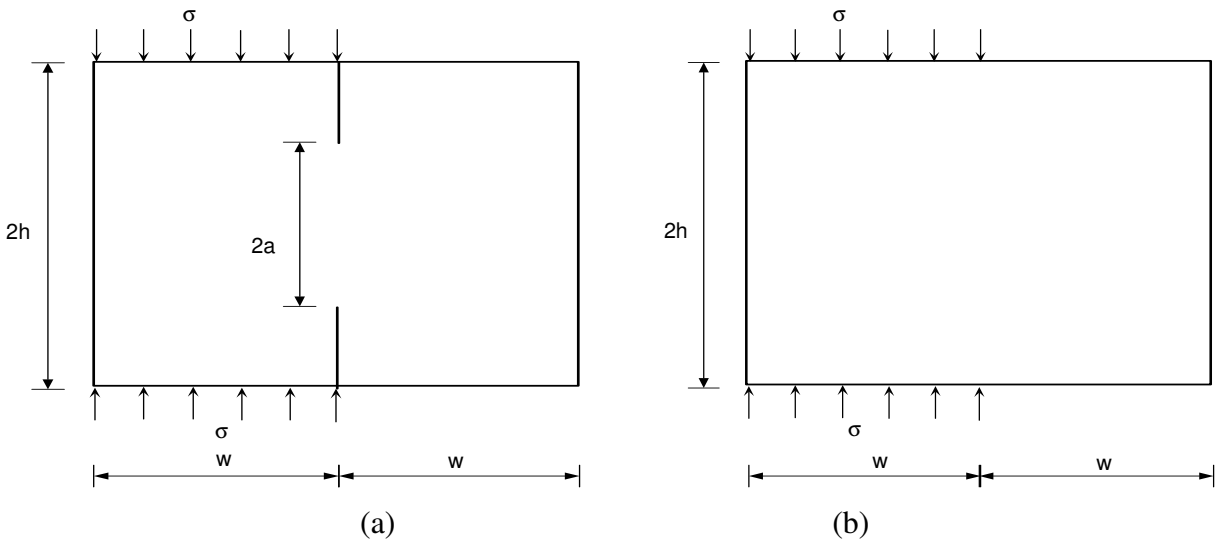

Figure 38. The same loading arrangement on two different specimens: (a) a notched specimen configuration; and (b) an unnotched specimen.

When the ligament lengths are different, a difference of the deformation energy could be experimentally measured. Using the difference, the fracture energy needed by driving the crack with a unit area can be determined. Generally, there are two ideal loading approaches to perform the tests. One is that the

boundary condition of deformation is given. The other is that the applied load to the two specimens shown is the same.

If the boundary condition of deformation has been given in the tests, two load vs. displacement curves corresponding to the two different specimen configurations are illustrated in Figure 39.

The total work of load transforms mainly into three parts, besides thermal energy dissipation that can be neglected until the maximum load is reached. The first part transforms into the compressive strain energy. The plastic deformation and the slight compressive failure in the loaded part dissipate the second part. The third part is dissipated due to shear crack propagation along the ligament. According to the load vs. deformation plots measured at the unloaded part, the energy dissipation due to shear crack propagation along the ligament proceeds until the loading arrives at its maximum. Once the maximum load is exceeded, the dissipation of the work of load is predominantly due to the compressive failure in the loaded part.

Now we discuss two cases shown in Figure 39 and Figure 40 separately. In Figure 39 the boundary condition of deformation is given. The thickness of two kinds of specimens is the same and is denoted with b. The notch depth of the notched specimen is c. The above plot of load vs. displacement measured from the unnotched specimen is marked with curve 1 and the lower one that is measured from the notched specimen is curve 2. According to the definition of fracture energy by Hillerborg (1976) [48], the mode II fracture energy G_{IIF} can be evaluated as follows:

$$G_{IIF} = \frac{\Delta W}{2cb} = \frac{1}{2cb} \int_0^{\delta_p} [\, F_1(\delta) - F_2(\delta) \,] d\delta \tag{8}$$

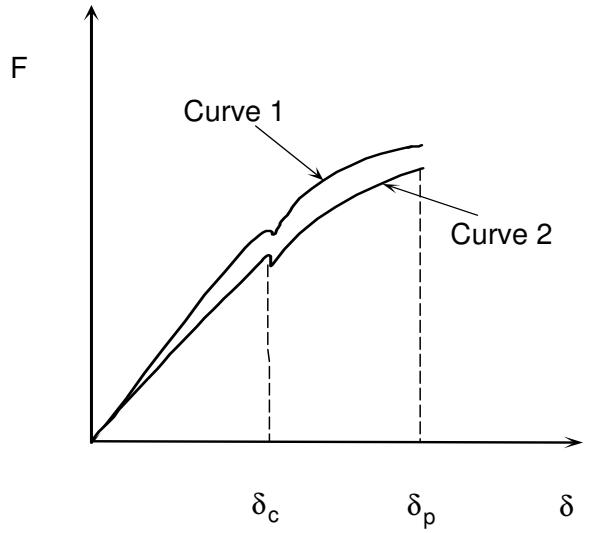

Figure 39. Illustration of plots of load vs. displacement for the tests that the boundary condition of deformation is given.

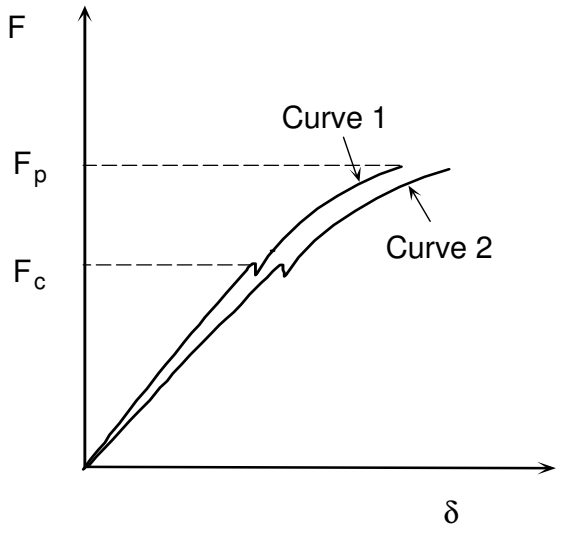

Figure 40 . Load vs. displacement plots for the tests with the same maximum loads.

In our tests, the specimens that have the same outline dimension, besides the ligament length, and are composed of the same concrete were tested under the same loading condition. The same loading arrangement, the same specimen dimensions and the same concrete led the approximately same maximum load. The difference of the ligament length led the different deformation. So, the measured plots of load vs. displacement presented in Figure 32 can be abstracted into the pattern shown in Figure 40 .

The mode II fracture energy G_{IIF} for the tests illustrated in Figure 40 can be calculated as follows:

$$G_{IIF} = \frac{\Delta W}{2cb} = \frac{1}{2cb} \int_0^{F_p} [\delta_2(F) - \delta_1(F)]dF \tag{9}$$

According to integration (9), if one knows the area between the curves 1 and 2 shown in Figure 40 , the mode II fracture energy G_{IIF} can be evaluated using the measured load vs. displacement plots. In fact, the difference ΔW between load work W_p is equal to that between residual work W^R_p corresponding to the peak load F_p. Considering such a fact that there is some deviation of practically measured load vs displacement plots from the ideal cases, a better way calculating the difference ΔW of load work between two specimens with different liga-

ment lengths is to evaluate the difference between residual work measured from them.

As shown in Figure 40 , curve 1 represents the load vs. displacement plot measured from the unnotched specimen and curve 2 does the notched specimen. The residual work WRp for the curves 1 and 2 can be evaluated as follows respectively:

$$W_{p1}^{R} = F_{p1}\ \delta_{p1} - W_{p1} = F_{p1}\ \delta_{p1} - \int_{0}^{\delta_{p1}} F_1\ (\delta)\ d\delta \quad (for\ \ unnotched\ \ specimen) \tag{10}$$

It is known that for load work the relation $W_{p1} > W_{p2}$ generally satisfies. Therefore, there is a relation of $W^{R}_{p2} > W^{R}_{p1}$ too. So, integration (8) can be simply expressed as follows:

$$W_{p2}^{R} = F_{p2}\ \delta_{p2} - W_{p2} = F_{p2}\ \delta_{p2} - \int_{0}^{\delta_{p2}} F_2\ (\delta)\ d\delta \quad (for\ \ notched\ \ specimen) \tag{11}$$

$$G_{IIF} = \frac{\Delta W}{2cb} = W_{p2}^{R} - W_{p1}^{R} \tag{12}$$

The mode II fracture energy G_{IIF} gained according this approach in the experiments is presented in Table 4. For normal strength concrete, mode I fracture energy is about 80 N/m to 100 N/m. From the testing results shown in Table 4, mode II fracture energy is about 20 times to 25 times mode I fracture energy.

An average value of K_{IIc} from the two specimens DC30-1 and DC30-2 is 2.56 MPa $m^{1/2}$ that was calculated using formula (1). According to the relation of $G = K^2/E$, the critical energy release rate G_{IIc} in mode II is 240 N/m where the modulus of elasticity of the concrete was evaluated according to the compressive strength. To compare G_{IIc} with G_{IIF} in Table 4, the mode II fracture energy G_{IIF} is 8.6 times mode II critical energy release rate G_{IIc}. The ratio is the same amount as that in mode I.

Figure 29 and 30 and Table 4 show that the testing results gained in the experiments almost have no disparity due to good controlling of concrete quality and carefulness during testing procedure. However, more specimens need to be studied in the future.

Table 4. Fracture energy G_{IIF} and critical energy release rate G_{IIc} from mode II concrete fracture tests.

Specimen	F_c (kN)	δ_c (mm)	F_p (kN)	δ_p (mm)	Residual work W^R_p (N.m)	ΔW (N.m)	G_{IIF} (N/m)
DC30-1	319	0.460	422	0.649	129.78	12.35	2058
DC30-2	309	0.445	426	0.652	132.77		
Average	**314**	**0.453**	**424**	**0.650**	**131.27**		
DC0-1	320	0.420	420	0.599	118.62		
DC0-2	322	0.416	422	0.683	119.30		
Average	**321**	**0.418**	**421**	**0.641**	**118.92**		

6. SHEAR FRACTURE OF REINFORCED CONCRETE BEAMS WITHOUT STIRRUPS

In last two decades the experimental investigations focused on shear failure of reinforced concrete beams have been intensively performed by many researchers for capturing the failure mechanisms [49-66]. As the consequence, various shear failure models were proposed to attempt acquiring adequate formulae to predict the shear strength of the reinforced concrete beams with good accuracy for designing engineers. However, the formulae that are used in various design codes are empirically yet [67-72] inasmuch as no physically sound analytical mode that enables to yield satisfactory results for all cases of the shear failure of the reinforced concrete beams exists.

Recent years, some researchers have put their attentions on application of fracture mechanics to the shear failure of the reinforced concrete beams without stirrups for developing an analytical model with soundly physical fundament [63-66]. This is based on such a fact revealed in the intensively experimental investigations that the shear failure of a beam is triggered off by a series of fracture processes occurred in the beam. It is investigated that these fracture phenomena includes diagonal shear fracture of concrete in the web region, shear-compression fracture of concrete in the region above the tip of the critical crack, interface bond fracture between steel bar and concrete due to the shear stress concentration and splitting fracture of concrete cover. The later mentioned two fractures somehow lead to lost of the dowel action so called. In this section, we

will briefly introduce the some empirical methods used in several current designing codes; then, in details, introduce the fracture mechanics approaches to predict the shear failure of reinforced concrete beams without stirrups proposed by other researchers; finally, a physically sound analytical formula termed in mode II fracture toughness K_{IIc} of concrete materials that we recently achieved using fracture mechanics approach is presented.

6.1 Empirical approaches

As the mentioned above, inasmuch as the mechanism of shear failure of reinforced concrete beams without stirrups is very complex, no analytical model was developed for the use of current design codes for practical engineers. However, intensive experiments on reinforced concrete beams without stirrups have been carried out by many researchers and a lot of experimental data has been accumulated for appearances of various empirical formulae using phenomenological study approach, dimensional analysis and regression analysis.

However, according to intensively experimental observations and the conventional opinion of view, the shear transfer capacity of the reinforced concrete beams without stirrups is regarded as to be influenced by the five facts which are shear stresses distributed on the compression zone of concrete, arching action formed by the inclined compression force in the compression zone, aggregate interlock that enables to transfer the shear stress along the diagonal shear crack, the softening cohesive stress vertically distributed across the diagonal shear crack and the dowel action due to the longitudinal reinforcement. In spite of several models with somehow physical meaning, like the modified compression field theory (MCFT)[55] and truss models with concrete ties[57], were proposed; the corresponding calculation formulae are empirically formed using regression analysis of experimental data. Due to lack of the physically analytical model, various calculation formulae that are coded in the current design codes in the world wide are empirically using regression analysis of the experimental data. Currently, ACI Subcommittee 445-F is making a new proposal [73] to present an empirical formula to predict the shear capacity of the reinforced concrete beams without stirrups using a regression analysis of the experimental data based on the Evaluation Shear Database (ESDB) developed by the subcommittee. If one sees the empirical formulae used in the design codes, it can be found that the strength of concrete where it is in term of tensile strength appeared in a form of being approximately proportional to $\sqrt{f_c}$, the longitudinal reinforcement

ratio and the shear span-depth ratio were considered as the main influence facts on the shear capacity of the reinforced concrete beams without stirrups.

As an instance, we can see a basic form of earlier empirical formula proposed by Zsuty in 1968 [50] using the data of 86 reinforced concrete slender beams without stirrups which was constructed through a dimensional analysis and a regression analysis as follows:

$$V_c = 2210\left(f_c \rho \frac{d}{a_s}\right)^{1/3} bd \tag{13}$$

Where the unit of the critical shear bearing capacity V_c is kN, $\rho = A_s/bd$ longitudinal reinforcement ratio, a_s/d is the shear span-depth ratio, f_c is compression strength of concrete in MPa, the width b and the depth of beam d are in unit of m.

Furthermore, many experimental results show that there is size effect on shear capacity of the reinforced concrete beams. Therefore, the size effect on shear capacity has been considered in the British design code [68], the CEB-FIP Model Code 1990 [69], the Canadian Standards Association Model Code (CSA Code) [70] and the concrete design code of Japan (JSCE Code) [72].

Inasmuch as the formula used in CSA code [70] is based on the Modified Compression Field Theory (MCFT)[55], in addition to the difficulty of the method in practical use, when the depth d is quite large, the formula shows an over strong asymptotic size effect $V_c \sim d^{-1}$, which is contrary to the well-known knowledge that exponent -1/2 is the strongest size effect possible for the fracture mechanics size effect (Bazant and Yu 2003)[63]. The formulae that is gained using the MCFT approach are shown as follows:

$$V_c = \frac{245}{1275 + s_e}\sqrt{f_c}\, bd \quad \text{(mm and MPa units)} \tag{14}$$

$$s_e = \frac{35 s_x}{(a + 16)} \quad \text{(mm unit)} \tag{15}$$

Where, s_x is proportional to the depth d. For example, s_x is taken as 0.9d for the beams with concentrated reinforced near the tension face. This reveals the size effect with an exponent -1.

The corresponding formula used in JSCE Code [72] was proposed by Okamura and Higai (1980)[51] using the weakest link assumption according to Weibull's statistical theory (1939) [74].

The formulae proposed by the British code [68] and the CEB-FIP Model Code 1990 [69] were developed using much more experimental data from the basic form of the empirical formula of Zsuty[50].

Differently, the British design code did not consider the shear span-depth ratio a_s/d shown in following equation [68].

$$V_c = \frac{790}{\gamma_m}(100\rho)^{1/3}\left(\frac{0.4}{d}\right)^{1/4}\left(\frac{f_c}{25}\right)^{1/3} bd \tag{16}$$

Where, γ_m is a safety factor being 1.25 and $100\rho < 3$, V_c is kN, f_c is MPa, b and d are in m.

As the most sophisticated formula in the current design codes in the world wide, the formula proposed by the CEB-FIP Model Code [69] is as follows:

$$V_c = 150\left(1+\sqrt{\frac{0.2}{d}}\right)\left(\frac{3d}{a_s}\right)^{1/4}(100\rho)^{1/3} f_c^{1/3} bd \tag{17}$$

Where, V_c is kN, f_c is MPa, b, d and a_s are in m. It can be seen that the size effect is presented by an expected exponent -1/2 in formula (17).

Different from the aforementioned codes, ACI 318-89 code [67] proposed a simplified formula that the shear capacity is assumed to be entirely contributed by concrete.

$$V_c = \frac{1}{6}\sqrt{f_c}\, bd \tag{18}$$

Where, the unit of V_c is N, f_c is MPa, b and d are mm. However, it was found that formula (18) cannot predict the experimental results that the shear strength of the reinforced concrete beams without stirrups decreases as the depth of the beam decreases and the longitudinal reinforcement ratio decreases. Especially, when the size of the members is larger and is lightly reinforced, formula (18) will lead to an overestimated predication result. Therefore, the ACI subcommittee 445F [73] is working to propose a new proposal for adding new terms to attempt to reflect the influence of the size effect, the longitudinal rein-

forcement and the shear span-depth ratio on the shear capacity. The subcommittee has provided three empirical formulae for three different considered facts for choice. In the three empirical formulae, an exponent -1/3 is used for size effect that is not ideal according to fracture mechanics. An exponent -1/2 should be expected to be adopted for predicting size effect once the foregoing formulae would be improved using the concept of fracture mechanics. As the results, the corresponding coefficients used in the aforementioned formulae should be refitted according to the experimental data.

6.2 Fracture mechanics approaches

It was recognized that the shear failure of reinforced concrete beams is a very complex brittle fracture process and behaves significant size effect. Besides the various empirical formulae, the existing models with somehow physical meaning based on such intensive experiments on the shear failure of the reinforced concrete beams without stirrups carried out by many researchers only capture a little of interpretation for the shear mechanisms both in physics and mathematics. It motivated many researchers putting their attentions on application of fracture mechanics into shear failure of reinforced concrete beams without stirrups to attempt a physically sound analytical model.

Among the research works appeared in the last two decades, there mainly are two research objects that can be distinguished. One put an emphasis on predication of size effect of shear capacity of the reinforced concrete beams without stirrups. Another did on good interpretation of failure mechanisms.

Bazant developed a size effect formula from fracture mechanics for predicting the shear strength in 1984 [53]. In addition, Bazant and Kim (1984) [54]studied the size effect in shear failure of reinforced concrete beams using the size effect approach. In the work, the shear strength is assumed to be mainly due to a common contribution of the arching action and the composite beam action. Latterly, the size effect formula was extended by Bazant in 1987[56] to such a case that the cohesive stresses across the diagonal shear crack remain a limited residual value, do not decrease to zero, based on the concept of the cohesive crack model (i.e. fictitious crack model) that was proposed by Hillerborg in 1976[48].

Little later, Gustafsson and Hillerborg (1988) [59] numerically studied the diagonal shear cracking processes with different crack patters in RC members without stirrups using the fictitious crack model, of which, the main aim is to

investigate how predict the size effect of shear strength of the members. In the study, not only the size effect, but also the longitudinal reinforcement ratio and the shear span-depth ratio were investigated in details. As the result, they adopted the size effect formula of shear strength of RC beams without stirrups in a form of $d^{-1/4}$.

In this year (2003), Bazant and Yu [63] presented a new formula to predict the size effect of shear capacity of RC members without stirrups. According to the small- and large-size second-order asymptotic properties of the cohesive crack model gained by using dimensional analysis, a general form of the size effect with the same form as the previous work of Bazant was revealed once again that is presented as follows:

$$V_c = \beta \sqrt{\frac{f_c}{1 + d / d_0}} \tag{19}$$

Where, β and d_0 are two constants. Using a statistical regression based on the meticulously chosen experimental data with sound size effect from the data-base collected by ACI 445, the two constant parameters β and d_0 were determined for two different cases considering the influence of shear span-depth ratio a_s/d and without consideration of a_s/d respectively. They are shown as follows.

When the shear span-depth ratio is not considered, the two constants are given as follows:

$$d_0 = 30930 \left(\frac{\rho}{f_c} \right)^{2/3} \qquad \beta = 0.415 \text{ (mean)}, \beta = 0.315 \text{ (design)} \tag{20}$$

And, if the shear span-depth ratio is included, they are in formula (21).

$$d_0 = 37280 \left(\frac{\rho}{f_c} \right)^{2/3} \left(\frac{d}{a_s} \right)^{1/3} \qquad \beta = 0.457 \text{ (mean)}, \beta = 0.35 \text{ (design)} \tag{21}$$

In the foregoing formulae, V_c and f_c are MPa, in SI units and d, a_s are in mm, ρ is a number, not a percentage.

In order to better understand the shear failure mechanisms of the reinforced concrete members without stirrups, Jenq and Shah (1989) [64] employed the two-parameter fracture model to analyses the diagonal shear crack. In their study, the shear capacity is assumed to be a combination contribution of the

concrete and the longitudinal reinforcement. In this way, the steel action associates with the bond stress which is assumed to be function of the embedded length. Later, Karihaloo (1993) [65] made a modification for Jenq and Shah's model [64] by taking into account the bond-slip relationship, the dowel action and the aggregate interlock.

Recently, Gastebled and May (2001) [66] proposed an analytical model for the shear failure of the RC beams without stirrups using a fracture energy approach. As the consequence, they archived an analytical formula that agrees very well with the empirical formula of the CEB-FIP Model Code 1990. Using this formula, one can predict the shear bearing capacity of the reinforced concrete beams without stirrups by taking into account the size effect, shear span-depth ratio, the longitudinal reinforcement ratio, the elastic modulus of steel and the concrete strength. Herein, we will introduce their shear fracture model in details to show how use fracture mechanics approach to predict the shear failure of the reinforced concrete beams without stirrups.

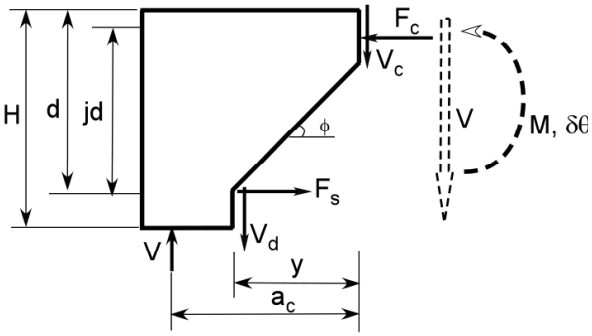

Figure 41. The free body illustration.

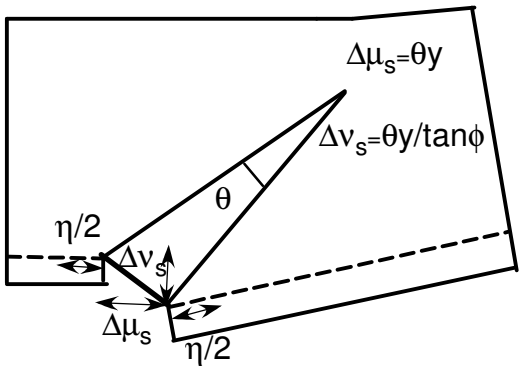

Figure 42. Detailed illustrations of steel bar deformation and geometry assumed.

The main principle used in Gastebled and May's approach [66] is that the unit extra work produced by the extra moment to the unit rotation at the tip of diagonal shear crack is equal to the fracture energy that is necessary to extend the unit unbonded length of longitudinal reinforcement. In fact, the unbounded failure could be dominated by a mode II fracture caused by high concentration of the bond stress on the interface between the steel and the concrete.

The free body diagram used in the paper of Gastebled and May (2001) [66] is shown in Figure 41. The detail of the steel deformation after unbonded is illustrated in Figure 42. If the angle of the diagonal shear crack is assumed to be 45°, the horizontal component F_s and the vertical F_d of the internal force in the longitudinal reinforcement crossing the diagonal shear crack are assumed to be associated with the angle of rotation θ at the tip of the diagonal shear crack according to the elastic properties of the steel and the deformation coordination conditions. The corresponding equations are given as follows:

$$F_s = \frac{E_s A_s}{\eta} \Delta u_s = \frac{E_s A_s}{\eta} y\theta \tag{22}$$

$$F_d = \frac{G_s B_s}{\eta} \Delta v_s = \frac{9}{26} \frac{E_s A_s}{\eta} y\theta \tag{23}$$

Where, E_s and G_s are the elastic modulus and the shear modulus of the steel respectively and they meet a relation of $G_s = E_s / (2(1+\nu_s) = 9\ E_s /26$ for engineering application. A_s represents cross section area of the longitudinal steel bar. Under shear condition, the calculated area of the cross section should be reduced, assuming $B_s = 0.9\ A_s$. η is the unbonded length of the steel.

According to the equilibrium conditions of the free body shown in Figure 41, one can get the following set of equations:

$$F_s = F_c \tag{24}$$

$$V = V_c + V_d \tag{25}$$

$$V\ a_c = yV_d + jd\ F_s \tag{26}$$

If the horizontal projection length y of the diagonal crack and the internal moment arm jd are assumed to be proportional to the height of the beam H, there are y = qH and jd = rH. Then, submitting equations (22) and (23) into equation (26), we have equation (27).

$$V\ a_c = q(\frac{9}{26}q + r) \frac{E_s A_s}{\eta} H^2 \theta \tag{27}$$

If θ is considered as a function of variable η and a differentiation for function θ is made refereeing to the variable η, one can set up a differentiation equation as follows:

$$\delta\theta = \frac{a_c}{A_s E_s} \frac{V}{q(9q/26+r)H^2} \delta\eta \tag{28}$$

Where, δη is the variation of the unbonded length.

According to the linear elastic fracture mechanics, the variation rate of the extra work is 2 times the energy variation at the critical fracture state, it is presented as following fundamental equation:

$$\delta W = 2\delta G \tag{29}$$

For considering the energy equilibrium at the critical fracture state in the unbonded failure shown in Figure 41, we have the following equation.

$$a_c V_c \delta\theta = 2G\delta\eta \tag{30}$$

Where, G is the fracture energy necessary to drive the crack propagation of unit length which is equal right unit unbonded length of steel bar.

Formula (30) applies to the unit thickness case. If we want to know the shear bearing capacity of a beam with thickness b, the thickness b must be considered in next analytical derivation. Additionally, the foregoing bond fracture is mode II fracture domination case, not mode I fracture. According to the conventional definition, the fracture energy is necessary to create a unit area of crack propagation. Therefore, now we should use the term G_{IIF} that represents mode II fracture energy to create unit area of crack, instead of the symbol G that is the fracture energy to create unit length of crack for the unit thickness case shown in formula (30). As the consequence, the corresponding expression of critical shear capacity of a reinforced concrete beam without stirrups can be obtained by submitting equation (28) into equation (30) as follows:

$$V_c^2 = \left(\frac{qH}{a_c}\right)^2 \left(\frac{9}{13} + \frac{2r}{q}\right) A_s E_s G_{IIF} b \tag{31}$$

In the work, Gastebled and May (2001) [66] assumed q= 0.8 and r=0.9 according to the shear capacity properties of reinforced concrete beams without stirrups. Then, we have following expression.

$$V_c = 1.372 \frac{H}{a_c} \sqrt{b G_{IIF} A_s E_s} \tag{32}$$

In order to predict the position of diagonal crack a semi-empirical formula that had been proposed by Kim and White (1991) [61] is given as follows:

$$a_c = 3.3 a_s \left(\frac{\rho (d / a_s)^2}{\left(1 - \sqrt{\rho}\right)^2} \right)^{1/3} \tag{33}$$

When equation (33) is submitted into equation (32) and let d= 0.9H, the equation for predicting the shear capacity of the reinforced concrete beams without stirrups can be expressed as follows:

$$V_c = \frac{0.446}{\sqrt{H}} \left(\frac{H}{a_s} \right)^{1/3} \rho^{1/6} (1 - \sqrt{\rho})^{2/3} \sqrt{E_s} \sqrt{G_{IIF}}\, bH \tag{34}$$

Due to lack of mode II fracture energy measured form tests, Gastebled and May [66] directly used mode I fracture energy G_f submitting into equation (34), instead of G_{IIF}. According to CEB-FIP Model Code 1990 [69], the mode I fracture energy is estimated using the following equation:

$$G_f = (0.0469 d_{agg} - 0.5 d_{agg} + 26) \left(\frac{f_c}{10} \right)^{0.7} \qquad \text{N.m/m}^2 \tag{35}$$

Let d_{agg} = 0.02 m, the above equation can be expressed a simple form.

$$G_f = 5.2 f_c^{0.7} \qquad \text{N.m/m}^2 \tag{36}$$

Submitting (36) into (34), we can once again get the analytical formula to predict the shear capacity of reinforced concrete members without stirrups achieved by Gastebled and May (2001) [66]. However, the coefficient is little different.

$$V_c = \frac{1.016}{\sqrt{H}}\left(\frac{H}{a_s}\right)^{1/3} \rho^{1/6}(1-\sqrt{\rho})^{2/3} f_c^{0.35}\sqrt{E_s}\, bH \quad \text{(N, mm, MPa, GPa units)} \quad (37)$$

After comparing with the empirical formula proposed by CEB-FIP Model Code 1990 [69], it was found that the formula (37) has good agreement with that of CEB-FIP Model Code 1990. It means that fracture mechanics can be employed as a useful tool to analyse the shear fracture of reinforced concrete members without stirrups.

Using a basic fundament of linear elastic fracture mechanics, there is a relationship of $K_{IIc} = (G_{IIF}\, E_c)^{1/2}$. Then, considering a relationship between the elastic modulus of the steel and the concrete, the equation (34) could be expressed as follows.

$$V_c = 1.372\sqrt{\frac{E_s}{E_c}}\frac{1}{a_c}\sqrt{\rho H}\, K_{IIc} bH \quad (38)$$

By the way, the equation that associates with mode II fracture toughness K_{IIc} of concrete can be deduced by submitting equation (33) into equation (38) and let d= 0.9H. The equation for predicting the shear capacity of the reinforced concrete beams without stirrups in terms of mode II fracture toughness K_{IIc} can be expressed as follows:

$$V_c = \frac{0.446}{\sqrt{H}}\sqrt{\frac{E_s}{E_c}}\left(\frac{H}{a_s}\right)^{1/3} \rho^{1/6}(1-\sqrt{\rho})^{2/3} K_{IIc}\, bH \quad \text{(N, mm, N/mm}^{3/2}\text{ units)} \quad (39)$$

Theoretically specking, we would prefer to use formula (39) for predicting the shear strength of RC members without stirrups. It needs to perform intensive mode II fracture tests to know the mode II fracture toughness K_{IIc} or mode II fracture energy G_{IIF} of concrete materials with different strength scales and the design values of K_{IIc} or G_{IIF} which correspond to 5% probability cut-off.

When $E_s/E_c = 6$ is used, equation (39) can be simplified as follows. In assessment of shear capacity of RC beams without stirrups, a larger safety factor $\gamma_m = 1.35$ is assumed considering mode II fracture toughness as a new material property.

$$V_c = \frac{1.09}{\gamma_m \sqrt{H}} \left(\frac{H}{a_s} \right)^{1/3} \rho^{1/6} (1 - \sqrt{\rho})^{2/3} K_{IIc} bH \qquad \text{(N, mm, N/mm}^{3/2}\text{ units)} \quad (40)$$

Now we could use some date as an example to calculate the shear strength using formulae (40), (37) to compare with the corresponding results using the formulae of the CEB-FIP Model Code and the ACI 318-89. In the calculations, f_c = 30 MPa, ρ = 0.02, d = 500 mm, H = 555 mm, a_s/d = 2, K_{IIc} = 1.2 MPam$^{1/2}$ = 38 N/mm$^{3/2}$ are assumed. The shear stresses calculated using the aforementioned formulae are given in Table 5.

It could be concluded that fracture mechanics applies to the prediction of shear bearing capacity of reinforced concrete members without stirrups. It provides a new tool to get analytical formula for shear fracture problems in reinforced concrete members.

Table 5. The shear stresses calculated using several formulae.

Formulae used	ACI 318-89	CEB-FIP	Formula (37)	Formula (40)
Shear stresses (MPa)	0.913	0.650	0.776	0.745

7. CONCLUSIONS AND DISCUSSIONS

As well known, there are no valid analytical formulae in current various design codes as the shear facture in concrete and reinforced concrete members are very complex. Many experimental observations show that shear fracture happened in concrete and reinforced concrete members without stirrups are brittle, which prompted that many researchers have attempted to use fracture mechanics as analytical tool for predicting the shear bearing capacities of both the concrete members and the reinforced concrete members without stirrups. Their investigation results show that fracture mechanics applies shear fracture of both concrete members and the reinforced concrete members. The several analytical models based on fracture mechanics proposed by some researchers reveal that these models not only can analytically predict the shear strength of reinforced concrete beams without stirrups, but also physically interpret the shear fracture mechanisms. The formulae (37) and (40) in section 6 deduced from the fundamental of fracture mechanical enable to accurately estimate the size effect in shear fracture, the contributions of the shear span-depth ratio, the reinforcement ratio and the concrete quality to shear strength. Due to mode II fracture domina-

tion in shear fracture both in a few cases of realist pure shear fracture in practical structures and in the shear fracture of reinforced concrete members, it needs to understand the shear fracture mechanics and shear fracture properties of concrete materials. Therefore, it is important to perform more mode II fracture tests for various concrete materials to know the mode II fracture toughness K_{IIc} and mode II fracture energy G_{IIF} of concrete materials with different strength scales.

In last two decades, many researchers have focused their attentions on seeking mode II fracture testing approaches to carry out mode II fracture tests without mode I component supplement. Their experimental investigation showed that it is very difficult to perform pure mode II fracture tests without mode I component supplement. In this chapter, we mainly introduced our developments on mode II fracture tests on double-edge notched specimens including theoretical analyses, numerical studies and experimental investigations. Using this new developed specimen geometry and loading arrangements, critical mode II stress intensity factor, i.e. mode II fracture toughness K_{IIc} of concrete materials were measured. The mode II fracture energy G_{IIF} is determined using a practical approach too. These results are beneficial for better understanding mode II fracture properties of concrete. Practically measured mode II fracture parameters introduced in sections 4 and 5 provide sufficient supports for the efforts on applying fracture mechanics to shear fracture of reinforced concrete members without stirrups introduced in section 6. Comparing with intensive fracture tests, mass accumulation of experimental data and good understanding for mode I softening properties of the fracture process zone and the crack propagation investigations for mode I crack in concrete materials, both on understanding for fracture mechanisms and practical experiments on mode II fracture tests on concrete materials are not enough. It is expected that more mode II fracture tests for concrete materials and more researches on development of fracture mechanics model to predict shear fracture of reinforced concrete members will be performed in more laboratories in the future.

REFERENCES

1. Iosipescu, N. (1967), New Accurate Procedure for Single Shear Testing of Metals. **Journal of Materials**, Vol. 2, No. 3, pp 537-566.

2. Arrea, M. and Ingraffea, A.R. (1981), Mixed-Mode Crack Propagation in Mortar and Concrete. Department of Structural Engineering Report 81-13, Cornell University.

3. Bazant, Z.P. and Pfeiffer, P.A. (1986), Shear Fracture Test of Concrete. **Materials and Structures** (RILEM), Vol. 110, No. 19, pp 111-121.

4. Swartz, S.E. and Taha, N.M. (1990), Mixed Mode Crack Propagation and Fracture in Concrete. **Engineering Fracture Mechanics**, Vol. 35, No. 1/2/3, pp 137-144.

5. Swartz, S.E., Lu, L.W., Tang, L.D. and Refai, T.M.E. (1988), Mode II Fracture Parameter Estimates for Concrete from Beam Specimens. **Experimental Mechanics**, pp 146-153.

6. van Mier, J.G.M., Nooru-Mohamed, M.B. and Timmers, G. (1991), An Experimented Study of Shear Fracture and Aggregate Interlock in Cement based Composites. **HERON**, Vol. 36, No. 4, pp 1-104.

7. Ballatore, E., Carpinteri, A. and Ferrara, G. (1990), Mixed Mode Fracture Energy of Concrete, **Engineering Fracture Mechanics**, Vol. 35, No. 1/2/3, pp 145-157.

8. Barr, B. and Derradj, M. (1990), Numerical Study of a Shear (Mode II) Type Test Specimen Geometry. **Engineering Fracture Mechanics**, Vol. 35, No. 1/2/3, pp 171-180.

9. Schlangen, E. (1993), Experimental and Numerical Analysis of Fracture Processes in Concrete. **HERON**, Vol. 38, No. 2.

10. Mattock, A.H. and Hawkins, N.M. (1972), Shear Transfer in Reinforced Concrete-Recent Research. **ACI Journal**, pp 55-75.

11. Nooru-Mohamed, M.B., Mixed-Mode Fracture of Concrete: An Experimental Approach, Ph. D. thesis. Delft University of Technology, Delft, The Netherlands, 1992.

12. Tada, H., Paris, P. and Irwin, G. (1985), **The Stress Analysis of Cracks Handbook** (second edition). Paris Productions Incorporated, St. Louis.

13. Davies, J. (1991), Numerical and Experimental Study of Development of Fracture Path under Mixed Mode Loading. in **Fracture Processes in Concrete, Rock and Ceramics** (Edited by J.G.M. van Mier, J.A. Rots and A. Bakker), RILEM Proceedings 13, E & FN Spon, London.

14. Davies, J. (1995), Study of Shear Fracture in Mortar Specimens. **Cement and Concrete Research**, Vol. 25, No. 5, pp 1031-1042.

15. Luong, M.P. (1990), Tensile and Shear Strength of Concrete and Rock. Engineering Fracture Mechanics, Vol. 35, No. 1/2/3, pp 127-135.

16. Richard, H.A. (1981), A New Compact Shear Specimen. **International Journal of Fracture**, Vol. 17, No. 5, pp R105-R107.

17. Banks-Sills, L. and Arcan, M.(1983), An Edge-Cracked Mode II Fracture Specimen, Experimental Mechanics, Sept. pp. 257-261.

18. Izumi, M., Mihashi, H. and Humura, N. (1986), In Fracture Toughness and Fracture Energy of Concrete (Edited by F.H. Wittmann), Elsevier Science, Amsterdam, pp. 347-354.

19. Irobe, M. and Pen, S.-Y. (1992), Mixed-Mode and Mode II Fracture in of Concrete. in **Fracture Mechanics of Concrete Structures** (Edited by Z.P. Bazant), Elsevier Applied Science, London and New York, pp 719-726.

20. Jia, Z. and Shah, S. P. (1996), Cement and Concrete Research, vol. 26, pp. 125-137.

21. Jenq, Y. S. and Shah, S.P. (1988), International Journal of Fracture, Vol. 38, pp. 123-142.

22. Barr, B. and Thomas, W.F. (1986), A Study of the Fracture Characteristics of Glass Reinforced Cement. **Proc. Third Int. Symp. on Developments in FRC Composites**, Sheffield, England.

23. Barr, B. (1987), The Fracture Characteristics of FRC Materials in Shear. in **Fiber Reinforced Concrete Properties and Applications** (Edited by Shah and Baston), pp 27-53. American Concrete Institute, SP-105.

24. Barr, B., Hasso, A. and Khalifa, S.(1987), A Study of Mode II Shear Fracture of Notched Beams, Cylinders and Cores. **Proceedings, SEM-RILEM Int.**

Conf. on Fracture of Concrete and Rock (eds, S.P. Shah and S.E. Swartz), Houston, pp 370-382.

25. Bazant, Z.P. and Pfeiffer, P.A. (1985), Tests of Shear Fracture and Strain Softening in Concrete, **Proceedings of the 2nd Symposium on the Interaction of Non-Nuclear Munitions with Structures**, April 15-19, Panama City Beach, Florida.

26. Cramer, S. and Pugel, A. (1987), Compact Shear Specimen for Wood Mode II Fracture Investigations. **International Journal of Fracture**, Vol. 35, pp 163-174.

27. Davies, J. (1998), Experimental Study of Crack Propagation in the Modified Punch-through Shear Specimen in Mixed-Mode Loading. **Fracture Mechanics of Concrete Structures, Proceedings FRAMCOS-3**, Aedificatio Publishers, Freiburg, Germany, pp 761-771.

28. Davies, J. (1992), Macroscopic Study of Crack Face Bridging Phenomenon in Mixed-Mode Loading. in **Fracture Mechanics of Concrete Structures** (Edited by Z.P. Bazant), Elsevier Applied Science, London and New York.

29. Ingraffea, A.R. and Panthaki, M.J. (1985), Analysis of "Shear Fracture" Tests of Concrete Beams. **Finite Element Analysis of Reinforced Concrete Structures**, ASCE, Tokyo, pp.151-173.

30. Kumosa, M. and D. (1987), Hull, Mixed-Mode Fracture of Composites Using Iosipescu Shear Test. **International Journal of Fracture**, Vol. 35, pp. 83-102.

31. Liu, K., Barr, B. and Watkins, J. (1985), Mode II Fracture of Fibre Reinforced Concrete Materials. The **International Journal of Cement Composites and Lightweight Concrete**, Vol. 7, No. 2, pp 93-101.

32. Xu, Shilang, Reinhardt, H.W. and Gappoev, Murat (1996), Mode II Fracture Testing Method for Highly Orthotropic Materials Like Wood. **International Journal of Fracture**, Vol. 75, pp 185-214.

33. Reinhardt, Hans W., Ozbolt, Josko, Xu, Shilang and Dinku, Abebe (1997), Shear of Structural Concrete Members and Pure Mode II Testing. **Advanced Cement Based Materials**, vol.5, pp.75-85.

34. Ozbolt, J., Reinhardt, H.W. and Xu, S. (1998), Numerical Studies on the Double-Edge Notched Mode II Geometry. **Fracture Mechanics of Concrete Structures, Proceedings FRAMCOS-3**, Aedificatio Publishers, Freiburg, Germany, pp 773-782.

35. Cedolin, L., Bisi, G. and Narodello, P. (1997), Sulla Determinazione Sperimentale Dell'Energia di Fracttura in Modo II per il Calcestruzzo. **Studi e Ricerche**, Vol. 18.

36. Cedolin, L., Bisi, G. and Narodello, P. (1998), On the Detection of Crack Propagation in Reinhardt's Double-Edge Concrete Testing Specimen for Mode II. Dipartmento di Ingegneria Strutturale, Politecnico di Milano.

37. Prisco, M.di and Ferrara, L. (1998), On the Evaluation of Mode II Fracture Energy in High Stength Concrete. **Computational Modelling of Concrete Structures**, de Borst, Bicanic, Mang & Meschke(eds), Balkema, Rotterdam.

38. Reinhardt, Hans W. and Xu, Shilang (1998), Experimental Determination of K_{IIc} of Normal Strength Concrete. **Materials and Structures**, vol. 31, pp 296-302.

39. Reinhardt, Hans W. and Xu, Shilang (2000), A Practice Testing Approach to Determine Mode II Fracture Energy GIIF for Concrete. International Journal of Fracture, V. 105, No. 2, pp. 107-125.

40. Rice, J. R. (1968), A Path Independent Integral and the Approximate Analysis of Strain Concentrations by Notches and Cracks, Journal of Applied Mechanics, Vol. 35, No. 2, pp. 379-386.

41. Radaj, D. and S. Zhang, Stress Intensity Factors for Spot Welds Between Plates of Unequal Thickness. Engineering Fracture Mechanics, 1991, Vol. 39, No. 2, pp. 391-413.

42. Keer, L.M., Stress Analysis for Bonded Layers. Journal of Applied Mechanics, Sept. 1974, pp. 679-683.

43. Yahsi, O.S. and A.E. Gösmen, Contact Problem for Two Perfectly Bonded Dissimilar Infinite Strips. International Journal of Fracture, 1987, Vol. 34, pp. 162-177.

44. Keer, L.M. and Q. Guo, Stress Analysis for Symmetrically Loaded Bonded Layers. International Journal of Fracture, 1990, Vol. 43, pp. 69-81.

45. Keer, L.M. and Q. Guo, Stress Analysis for Thin Bonded Layers. Advance in Fracture Research, 1989, Vol. 4, pp. 3073-3080.

46. Ozbolt, J. Maßstabseffekt und Duktilität von Beton- und Stahlbeton-Konstruktionen. Habilitationsschrift, 1995, Stuttgart University, Stuttgart.

47. Ozbolt, J, Li Y., Kozar I., (2001), Microplane Model for Concrete with Relaxed Kinematic Constraint. Int. J. of Solids and Structures., 38, 2683-2711.

48. Hillerborg, A., Moder, M., and Petersson, P. E. Analysis of Crack Formation and Crack Growth in Concrete by Means of Fracture Mechanics and Finite Elements, Cement and Concrete Research, 6, 1976, pp. 773-782.

49. Leohardt, F., and Walther, R., Versuche an Plattenbalken mit hoher Schubbeanspruchung, Deutscher Ausschuss Stahlbeton, V.152, 1962.

50. Zsutty, T. C., Beam Shear Strength Prediction by Analysis of Existing Data, ACI Journal, Proceedings V. 65, N0. 11, Nov, 1968, pp. 943-951.

51. Okamura, H., and Higai, T., Proposed Design Equation for Shear Strength of R.C. Beams without Web Reinforcement, Proceedings of the Japanese Society of Civil Engineers, V. 300, 1980, pp. 131-141.

52. Reinhardt, Hans W. and Walraven, Joost C. (1982), Cracks in Concrete Subject to Shear. **Journal of Structural Division, ASCE**, Vol.108, pp. 207-224.

53. Bazant, Z. P., Size Effect in Blunt Fracture: Concrete, Rock, Metal, Journal of Engineering Mechanics, ASCE, Vol. 110, pp. 518-535.

54. Bazant, Z. P., and Kim, J.-K., Size Effect in Shear Failure of Longitudinal Reinforced Beams, ACI Structural Journal, V.81, No. 5, Sep.-Oct. 1984, pp. 456-468.

55. Vecchio, F. J. and Collins, M. P., Modified Compression Field Theory for Reinforced Concrete Elements Subjected to Shear. ACI Journal, Proceedings V. 83. No. 2, March-April, 1986, pp. 219-231.

56. Bazant, Z. P., Fracture Energy of Heterogeneous Materials and Similitude, in Fracture of Concrete and Rock (eds. Shah, S. P., and Swartz, S. E.), Society of Experimental Mechanics, 1987, pp. 390-402.

57. Al-Nahlawi, K. A., and Wight, J. K., Beam Analysis Using Concrete Tensile Strength in Truss Models, ACI Structural Journal, V.89, No. 3, May-June, 1992, pp. 284-289.

58. Chana, P. S., Analytical and Experimental Studies of Shear Failures in Reinforced Concrete Beams, Proceedings of the Institute of Civil Engineers, V. 85, 1988, pp. 609-628.

59. Gustafasson, P. J., and Hillerborg, A., Sensitivity in Shear Strength of Longitudinally Reinforced Concrete Beams. ACI Structural Journal, V.85, No. 3, May-June, 1988, pp. 286-294.

60. Collins, Michael P. and Kuchma Daniel, How Safe Are Our Large, Lightly Reinforced Concrete Beams, Slabs, and Footings, ACI Structural Journal, V.96, No. 4, July-August 1999, pp. 482-490.

61. Kim, W., and White, R. N., Initiation of Shear Cracking in Reinforced Concrete Beams with no Web Reinforcements, ACI structural Journal, V.88, No. 3, May-June. 1991, pp. 301-308.

62. Bazant, Z. P. and Kazemi, M. T., Size Effect on Diagonal Shear Failure of Beams without Stirrups, ACI Journal, Proceedings V.88, No. 3, May-June 1991, pp. 268-276.

63. Bazant, Z. P., and Yu, Qiang, Design Against Size Effect on Shear Strength of Reinforced Concrete Beams without Stirrups. Structural Engineering Report No. 03-02/A466s, Infrastructure Technology Institute, Department of Civil and Environmental Engineering, Northwestern University, Evanston, Illions, 2003.

64. Jenq, Y. S., and Shah, S. P., Shear Resistance of Reinforced Concrete Beams-A Fracture Mechanics Approach, Fracture Mechanics: Application to Concrete, SP-118, V. Li and Z. P. Bazant, eds., American Concrete Institute, Farmington Hills, Mich., 1989, pp. 237-258.

65. So, K. O., and Karihaloo, B. L., Shear Capacity of Longitudinally Reinforced Beams A Fracture Mechanics Approach, ACI structural Journal, V.90, No. 6, Nov-Dec. 1993, pp. 591-600.

66. Gastebled, Olivier J. and May Lan M., Fracture Mechanics Model Applied to Shear Failure of Reinforced Concrete Beams without Stirrups, ACI Structural Journal, V.98, No. 2, March-April, 2001, pp. 184-190.

67. ACI Committee 318, Building Code Requirements for Reinforced Concrete (ACI 318-95) and Commentary (ACI 318 R-95), American Concrete Institute, Farmington Hills, Mich., 1995, 369 pp.

68. British Standards Institution, Code of Practice for Design and Construction, 2nd Edition, BSI, London, 1997.

69. Comité Euro-International du Béton, CEB-FIP Model Code 1990, Redwood Books, Wiltshire, England, 1993, 437 pp.

70. CSA Committee A23.3, Design of Concrete Structures: Structures (Design)-A National Standard of Cannada, Canadian Standards Association, Rexdale, Ontario, Candada, Dec. 1994, 199 pp.

71. AASHTO LRFD Bridge Design Specifications and Commentary, 1st ed., American Association of State Highway and Transportation Officials, Washington, D.C., 1994,1091 pp.

72. Standard Specification for Design And Construction of Concrete Structures, Part I (Design). Japan Society of Civil Engineers, Tokyo, 1991.

73. Summary of Evaluation of Proposals for the "Quick Fix" for Reinforced Concrete Members without Transverse Reinforcement. Subcommittee 445-F "Beam Shear" of ACI-ASCE Committee 445 "Shear and Torsion". 2003.

74. Weibull, W., A Statistical Theory of the Strength of Materials, Proceedings of Royal Swedish Academy of Engineering Science, 1939, V. 151, pp. 1-45.